Development of biobased building blocks, polymers and coatings

Hermens, J. George H.

DOI:
10.33612/diss.348356282

3

A Sustainable Polymer and Coating System based on Renewable Raw Materials

This chapter has been accepted for publication:
Johannes G.H. Hermens, Thomas Freese, Mathieu L. Lepage, Georgios Alachouzos, Keimpe J. van den Berg, Niels Elders, Ben L. Feringa, *Green Chem.* 2022, DOI: 10.1039/D2GC03657F

Abstract

Paints and coatings are widely used in modern society and their current production is mainly dependent on the petrochemical industry. The establishment of processes using sustainable alternative monomers based on biorenewable resources, using exclusively biobased reagents and using green synthetic transformations are highly warranted for a more sustainable future. Herein, we report on a sustainable polymer and coating system based on the monomer methoxybutenolide; a biobased acrylate alternative. Methoxybutenolide and the comonomer dodecyl vinyl ether are synthesized from biobased platform chemicals using the environmentally benign synthetic transformations photooxygenation and vinylation. For the photooxygenation, a biobased photosensitizer was developed exerting high quantum yields. The monomers were copolymerized using biomass derived (photo)initiators to yield fully biobased polymers and coatings with properties comparable to acrylate based coatings.

3.1 Introduction

Over the past decades, increased efforts have been taken to advance chemical science to a sustainable future.[1, 2] Technologies revolved around biobased chemicals and synthesis methods adherent to the Twelve Principles of Green Chemistry have been developed to be less dependent on petrochemical based materials and processes.[3-5] In particular polymers and coatings,[6] used for preservation, protection and decoration of virtually all man-made materials used in society, are frequently based on olefin-derived acrylate monomers, *ergo* a multi-million scale production heavily dependent on fossil feedstock.[7] These facts, paired with the undesirable emission of CO_x and other greenhouse gases in the conversion of finite fossil fuel feedstocks into molecules of higher value, highly warrant the development of sustainable alternatives and greener synthetic procedures.[8, 9]

The coating industry successfully implemented the latter by invention of new technologies such as acrylic dispersions in emulsion polymerization,[10, 11] solvent-free radiation-cured acrylics[12] and acrylic powder coatings[13] as green alternatives to solventborne coatings. Besides the sustainable aspect of less environmental pollution, these innovations significantly contributed to reduced risk of health hazards and improved industrial occupational safety, strengthening the Responsible Care initiative.[14]

Now, development of alternative sustainable processes is generally led by strategies such as opening new biobased synthetic routes to commodity and specialty chemicals or through establishing novel biobased building blocks for the replacement of these chemicals.[15] Despite significant progress, major challenges pertain to the development of completely sustainable processes.[6] An integrated approach considering the use of biorenewable resources, biobased reagents, sustainable catalysis and green solvents is highly desired. The inherent higher

complexity of biorenewable resources allows for a magnitude of different pathways to unique platform chemicals with different functional groups, whereas the development of biobased alternatives might lead to unprecedented reactivity.[16] The exploration and progress in the field of Green Chemistry towards the utilization of biomass-derived building blocks to replace the non-sustainable acrylate monomers has been successfully attained. Recently, advances were made towards the development of acrylate alternatives, and the free radical polymerization thereof, derived from the platform chemicals levoglucosenone,[17] Tulipalin A,[18] itaconic acid,[19-21] itaconic anhydride[22], muconic acid,[23, 24] and levulinic acid.[25] Implementing these acrylate alternatives results in promising polymer properties such as higher glass transition temperatures, higher stability and post-polymerization functionalization.

Previously we have shown the development of an attractive acrylate alternative based on a butenolide motif, derived from the platform chemical furfural.[26] Furfural is converted quantitatively into the non-substituted acrylic acid alternative hydroxybutenolide via a [4+2] cycloaddition with singlet oxygen ($^1O_2$), which is generated *via* photosensitization. Hydroxybutenolide was readily converted into a set of various alkoxybutenolides (linear and branched) by heating it in the presence of the appropriate alcohol. The alkoxybutenolides were used in combination with comonomers as vinyl esters and in particular vinyl ethers to yield promising polymeric materials. High reaction rates were found for the combination of butenolides and vinyl ethers, hence a divinyl ether was chosen as a suitable crosslinker for the formation of coatings. UV-curing of the butenolide divinyl ether mixture led to excellent hard coatings with tunable material properties depending on the substituents at the butenolide, showing their effectiveness as acrylate replacements and high versatility for coatings.

Despite the merits of the various reported systems, the resulting biobased polymers often do not consist of 100% biobased carbon content due to the use of petrochemical derived comonomers, reagents for derivatization or additives.

In the design reported herein, we take an integrated approach, using renewable resources, sustainable transformations, solvents and reagents to develop methodology for an integrated biobased polymer and coating system containing a significant amount of biobased carbon. All components used, including catalysts and polymerization initiators, originate from platform chemicals that are readily derived from lignocellulosic biomass. We report on the monomers methoxybutenolide and dodecyl vinyl ether, derived from the biomass derived chemicals furfural[27] and dodecanol,[28] made in a sustainable fashion through catalytic photooxygenation and vinylation using calcium carbide, respectively. Building on the already sustainable photooxidation[29] of furfural to hydroxybutenolide, the photosensitizer was replaced by a biobased, blue-light activated counterpart derived from the top value added platform chemicals levulinic acid and hydroxymethylfurfural (HMF).[30] The free radical polymerization was then carried out using a biobased radical initiator ascaridole derived from natural oil

terpinene via photooxygenation,[31] in combination with a sustainable solvent gamma-valerolactone (GVL) derived from levulinic acid,[32] to ultimately yield fully biobased polymers in high conversions. Finally, using the same approach for dodecyl vinyl ether, a biobased crosslinker was synthesized from 1,4-butanediol.[33] Together with a vanillin-derived UV photoinitiator, methoxybutenolide and the biobased crosslinker were cured, which resulted in a hard, transparent and fully biobased coating. Overall, the strategy reported herein demonstrates the viability of a polymerization platform where all components are derived from sustainable sources (**Figure 1**).

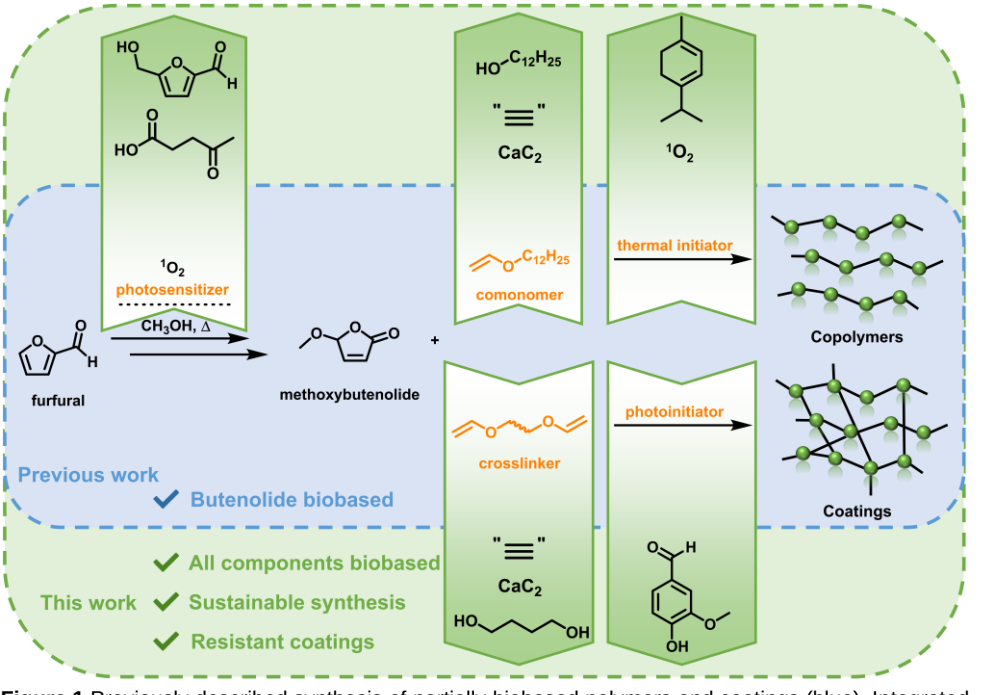

Figure 1 Previously described synthesis of partially biobased polymers and coatings (blue). Integrated biobased polymer and coating system with all components derived from biorenewable resources (green).

3.2 Results and Discussion

3.2.1 Photosensitizer

At the outset, to develop entirely biobased polymers and coatings, we sought to design a sustainable photosensitizer to transform furfural into hydroxybutenolide using catalytic photooxygenation with molecular oxygen, providing the precursor for the butenolide monomer. Recently, Mascal *et al.* described the synthesis of a biobased organic dye, which we will now refer as **FLY 450** (**Furan Lactone Yellow** with λ_{max} = 450 nm), with a high molecular absorptivity (ε) derived from the platform chemicals HMF and levulinic acid (**Figure 2A**).[34] We envisioned that such biobased lactone-substituted furans might well generate singlet oxygen under aerobic

irradiation, as similar organic dyes containing strong chromophores and high ε values often exhibit photosensitization properties.[35]

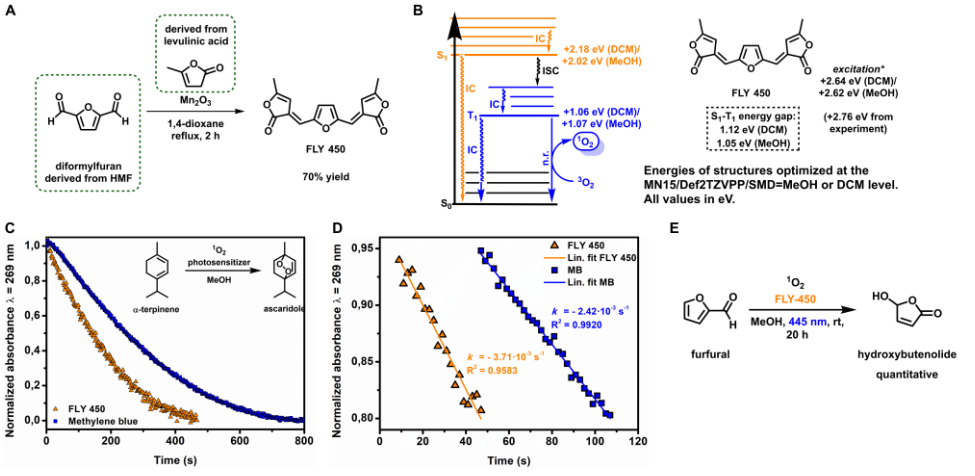

Figure 2 (A) Synthesis of FLY 450 from biobased chemicals diformylfuran and α-angelicalactone. (B) DFT/TD-DFT calculation results, conducted at the MN15/Def2TZVPP/SMD=DCM/MeOH level, from with the S_1-T_1 energy gap ΔE_{ST} was derived. (C) Decay of singlet oxygen scavenger α-terpinene, followed by UV-Vis spectroscopy in methanol at λ = 269 nm using FLY 450 (orange triangle) or methylene blue (blue square). (D) Rate of $^1O_2$ production (s^{-1}) of FLY 450 and methylene blue in methanol as a function of the decay of the scavenger, followed by UV-Vis spectroscopy at λ = 269 nm, determined from 95% to 80% conversion of scavenger using FLY 450 (orange triangle) or methylene blue (blue square). Photooxygenation conditions: α-terpinene (40 μM), photosensitizer (1 μM), pre-oxygenated methanol, 293 K, λ_{irr} = 445 nm. (E) Photooxidation of furfural employing FLY 450 (5 mol%) as photosensitizer yielding hydroxybutenolide quantitatively.

To interrogate the potential of such dyes, we turned to computational chemistry to predict the properties of **FLY 450**. We hypothesized that, in order for **FLY 450** to generate singlet oxygen upon irradiation, it must sufficiently populate its triplet T_1 excited state after intersystem crossing (ISC) from the singlet S_1 excited state initially accessed after absorption of a photon. Since the rate of ISC is inversely proportional to the obtained S_1-T_1 energy gap ΔE_{ST}, this value was examined using density functional theory (DFT) or time-dependent density functional theory (TD-DFT) methods.[36] The **FLY 450** S_0, S_1 and T_1 energies, as well as the vertical TD-DFT excitation energies were obtained at the MN15/Def2TZVPP/SMD=DCM or MN15/Def2TZVPP/SMD=MeOH level (**Figure 2B**, **Experimental Section Table S1**).[37-39] From these calculations we found promising ΔE_{ST} values of 1.12 eV (DCM) or 1.05 eV (MeOH), suggesting that ISC to the T_1 should be facile for both solvent systems. Notably, the lower ΔE_{ST} computed for more polar MeOH (due to a more stabilized S_1 state in simulated MeOH versus simulated DCM) suggests that one might predict fast intersystem crossing, and therefore strong photosensitization activity for **FLY 450** in polar, protic media. Known photosensitizer dyes (e.g. methylene blue), typically perform slightly better in less polar or aprotic media,[40] and these computational predictions encouraged us that **FLY 450** would indeed

exhibit high photosensitization activity, even in green solvents such as MeOH, or even with water as the co-solvent.

FLY 450 was synthesized in 70% yield *via* condensation of α-angelicalactone with diformylfuran (**Figure 2A**).[34] First, we were encouraged to find that the experimental values for the **FLY 450** absorption wavelength λ_{max} = 450 nm (+2.76 eV) were in very strong agreement with the computed vertical excitation energies of +2.78 or +2.79 eV, simulated DCM or MeOH, respectively (**Figure 2**). Next, in order to evaluate the oxygen photosensitization properties, **FLY 450** was applied in catalytic amounts (1 mol%) in the photooxidation of furfural to hydroxybutenolide in methanol using our previously described batch rotary photoreactor (see **Experimental Section Figure S3**).[26, 41, 42] To our delight, conversion towards the desired hydroxybutenolide was observed, experimentally confirming the computational predictions regarding the ISC rate, and thus also the photosensitization properties of **FLY 450**. The quantum yield (Φ_Δ), the efficiency of $^1O_2$ generation of this new photosensitizer, was determined by monitoring the decay of a $^1O_2$ scavenger over time by UV-Vis spectroscopy upon blue light irradiation (λ_{irr} = 445 nm). The rate of $^1O_2$ production is equal to the consumption rate of a scavenger, in our case the biobased oil α-terpinene, which is present in a large excess (40 eq.), as it is reasonable to assume every molecule of $^1O_2$ that is formed is captured. α-Terpinene is a diene that can undergo a [4+2] cycloaddition with $^1O_2$ to yield the stable endoperoxide ascaridole. Important for this study was that the absorption maxima of the scavenger α-terpinene (λ_{max} = 269 nm) and the resulting product ascaridole (λ_{max} = 205 nm) have no overlap and do not absorb in the visible light region where the photosensitizer **FLY 450** (λ_{max} = 450 nm) is excited (λ_{irr} = 445 nm) (**Experimental Section Figure S5**). The quantum yield of **FLY 450** in methanol and dichloromethane was derived from the ratio of scavenger decay rates, the photosensitizer absorptions at irradiation wavelengths and the reported quantum yields[43, 44] using methylene blue as a reference compound, according to a modified method from a published procedure (see **Experimental Section Figure S7– Figure S9**).[45] Using the rate determined between 5% and 20% conversion, the linear decay of α-terpinene (**Figure 2C, D**), the quantum yield for **FLY 450** in methanol was found to be $\Phi_\Delta = 0.22 \pm 0.02$, a high quantum yield value considering a small organic compound with no additional effects to enhance ISC (**Table 1**), such as the inclusion of ISC-accelerating heavy atoms. Similarly, in dichloromethane (DCM), a high quantum yield is observed for **FLY 450** ($\Phi_\Delta = 0.22 \pm 0.02$) (**Table 1**). It should be noted that due to the difference in molar extinction coefficient ε, a higher absolute rate of scavenger decay (i.e. a higher absolute $^1O_2$ production rate) is observed for methylene blue (**Table 1**). However, our newly designed biobased photosensitizer **FLY 450** exhibits excellent quantum yields (**Table 1**), particularly also in a greener alcoholic solvent (in this case, MeOH), signifying efficient singlet oxygen formation for sustainable applications.

Table 1 Photophysical properties of **FLY 450** and methylene blue in solution (1 µM, MeOH/DCM, 293 K). Quantum yields Φ_Δ reported as an average of a triplicate measurement.

Photosensitizer	Solvent	λ_{max} (nm)	ε ($M^{-1}cm^{-1}$)	Φ_Δ	$\Phi_\Delta \cdot$ ε ($M^{-1}cm^{-1}$)
FLY 450	**MeOH**	450	13139	0.22 ± 0.02	2917
	DCM	450	18305	0.22 ± 0.02	4085
Methylene blue	**MeOH**	654	50260	0.50[a]	25130
	DCM	654	27654	0.57[b]	15763

[a]Φ_Δ taken from literature.[43] [b]Φ_Δ taken from literature.[44]

Employing **FLY 450** as photosensitizer (5 mol%) in a batch photooxidation of furfural to hydroxybutenolide, full conversion to the desired product was achieved after 20 h (**Figure 2E**). After the reaction in methanol, we noticed discoloration of the solution, which suggested some photobleaching of our photosensitizer **FLY 450** was taking place. We hypothesized that as **FLY 450** contains an electron rich furan moiety, it should itself be inherently susceptible to [4+2] cycloadditions with $^1O_2$. Using a DFT thermochemistry approach we propose a decomposition pathway similar to the reaction mechanism of furfural towards hydroxybutenolide by formation of the endoperoxide and subsequent decomposition by the methanolic solvent (see **Experimental Section Figure S1**).

3.2.2 (Co-)monomer formation

With a sustainable synthesis towards hydroxybutenolide using our new biobased photosensitizer **FLY 450** for $^1O_2$ formation, the next step involved the derivatization, i.e. introduction of an alkoxy substituent. Previously we have shown the condensation of hydroxybutenolide with a variety of different alcohols allowing to tune the properties of the ultimate polymers.[26] Condensation reactions happen readily by heating in the absence of acid due to the unique tautomeric open form structure of hydroxybutenolide (**Figure 3A**). In the case of the low boiling point and environmentally attractive methanol,[46] hydroxybutenolide can be dissolved and heated at reflux in methanol to provide methoxybutenolide (76% yield), which was purified by distillation under reduced pressure giving us the first monomer (**Figure 3A**).

Vinyl ethers are well known monomers applied in a vast amount of polymer materials[47] and copolymerize particularly well with alkoxybutenolides, easily reaching full conversion under free radical polymerization in 2 h at 120°C.[26] For almost a century, the production of these useful comonomers, the vinylation of alcohols using acetylene, has been a well-established procedure.[48] Recently, calcium carbide as the source for acetylene has been increasingly explored and is nowadays considered a green and sustainable methodology.[49, 50] Calcium carbide is traditionally synthesized from coal in electric furnaces at elevated temperatures. Employing biochar, obtained from the pyrolysis of biorenewable resources, allows in addition to a biobased descent for shorter reaction times and lower, but still high (1700°C), working temperatures.[51] It is important to note that with biobased calcium

carbide, the original industrial Reppe Process of producing acrylic acid from acetylene, carbon monoxide and water could in theory become a sustainable technology. However, this reaction remains unattractive because of safety and pollution control problems arising from the formation of toxic side products.[7]

Aside from being derived from renewable feedstock, an additional advantage related to using calcium carbide is the ease of handling solids rather than gases. Alcohols, and even polyols like carbohydrates, are readily vinylated in closed vessels.[52-54] Fortunately, the vinylation of dodecanol (derived from natural oils like coconut and palm kernel oil)[28] gives us access to our previously reported comonomer, now made in a sustainable way. Using the previously reported optimal ratio of 1 to 4 (calcium carbide : water) dodecanol was converted to dodecyl vinyl ether and isolated in 73% yield (**Figure 3B**).

3.2.3 Free radical polymerization

With both biobased monomers in hand, we started with the free radical copolymerization of methoxybutenolide and dodecyl vinyl ether. Copolymerization using Trigonox 42S as thermal radical initiator ($t_{1/2}$ = 30 min at 120°C) in either 1-methoxy-2-propanol or butyl acetate as solvent (boiling points 120°C and 126°C, respectively) resulted in a 1:1 copolymerization with 95% conversion (see **Experimental Section Figure S10**). As the solvent is the major component (in weight) in the reaction, it is highly important to include it in the transition to fully biobased polymers and coatings. With careful consideration, GVL was chosen as a suitable solvent replacing butyl acetate or 1-methoxy-2-propanol. GVL is derived from levulinic acid and is used as a sustainable solvent (boiling point 205°C) and as a platform chemical for specialty chemicals and fuels.[32] Although the boiling point is considerably higher than its counterparts, GVL was employed here as green solvent for the copolymerization of methoxybutenolide and dodecyl vinyl ether, which resulted in a fast and full conversion of both of the monomers and a clean 1:1 copolymerization much to our delight (**Figure 3C, D** and **Experimental Section Figure S11**).

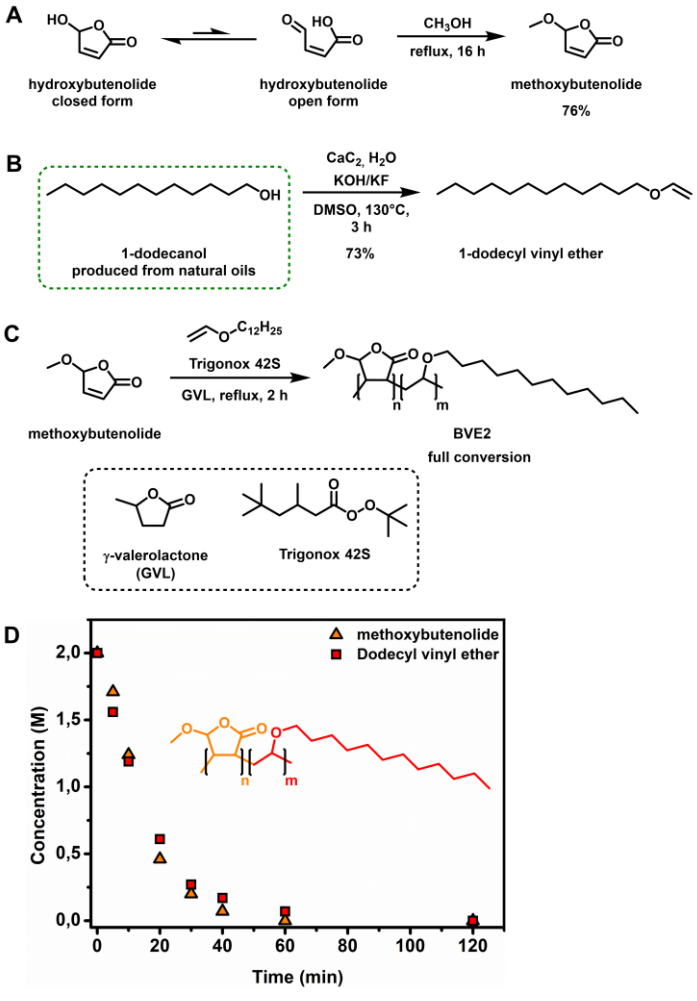

Figure 3 (A) Hydroxybutenolide equilibrium with the closed form as the dominant species and methanol condensation of the open form towards methoxybutenolide. (B) Vinylation of 1-dodecanol using calcium carbide.[47, 52-54] (C) Copolymerization of methoxybutenolide with dodecyl vinyl ether (1:1 ratio) in GVL using Trigonox 42S as radical initiator. (D) Concentration of monomers over time during the copolymerization of methoxybutenolide with dodecyl vinyl ether followed by ^{1}H NMR spectroscopy by taking samples and flash freezing (−18°C) them at certain timestamps using 1,3,5-trimethoxybenzene internal standard. Reaction conditions: monomers 2 M, Trigonox 42S (6 mol%), 1,3,5-trimethoxybenzene 0.5 eq., 120°C, 2 h.

Although a minor component in terms of carbon content in the resulting polymer chain, we sought to replace the radical initiator with a biobased alternative in order to obtain all components in a biobased fashion. Intrigued by the structure of the singlet oxygen scavenger product from our quantum yield determination studies (**Figure 2**), ascaridole, we envisioned that the thermal cleavage of the endoperoxide could initiate the copolymerization of a butenolide-vinyl ether mixture. To the best of our knowledge, only one example of free radical polymerization of methacrylonitrile initiated by thermal decomposition of ascaridole is known.[55] We

performed the larger scale synthesis and isolation of the endoperoxide using the previously described rotary photoreactor (**Figure 4A**, **Experimental Section Figure S3).**[26, 41, 42] In order to elucidate the stability of ascaridole, the thermal decomposition was studied at different temperatures. Based on an initial DFT thermochemistry prediction of the O-O bond homolytic cleavage of Trigonox 42s and ascaridole (see **Experimental Section Figure S2**), we calculated the thermal stability of ascaridole as a radical initiator was higher than Trigonox 42S (**Figure 4B**), suggesting that elevated temperatures would be required to obtain similar half-life times for radical initiation. Taking advantage of the higher boiling point green solvent GVL, ascaridole was dissolved in GVL (0.5 M) and heated at 140°C and 150°C, while the conversion was followed over time using ^{1}H-NMR spectroscopy by taking samples at regular intervals. As the thermal decomposition follows pseudo first-order reaction kinetics, due to radical formation followed by presumably radical transfer reactions to the solvent, a linear relation between conversion and time at a given temperature is found (**Figure 4B**). At 140°C, a rate constant was revealed that resulted in a half-life time of 45 min. The measured half-life for the decomposition of ascaridole was compared to that of Trigonox 42S in GVL (**Figure 4B**, red diamonds). Our comparison revealed a half-life of 29 min that corresponds to the literature value,[56] validating our measurements and our DFT thermochemistry predictions. At 150°C, the half-life of ascaridole was significantly decreased to 17 min, which suggests unfavorable termination reactions in the free radical polymerization process might be taking place.

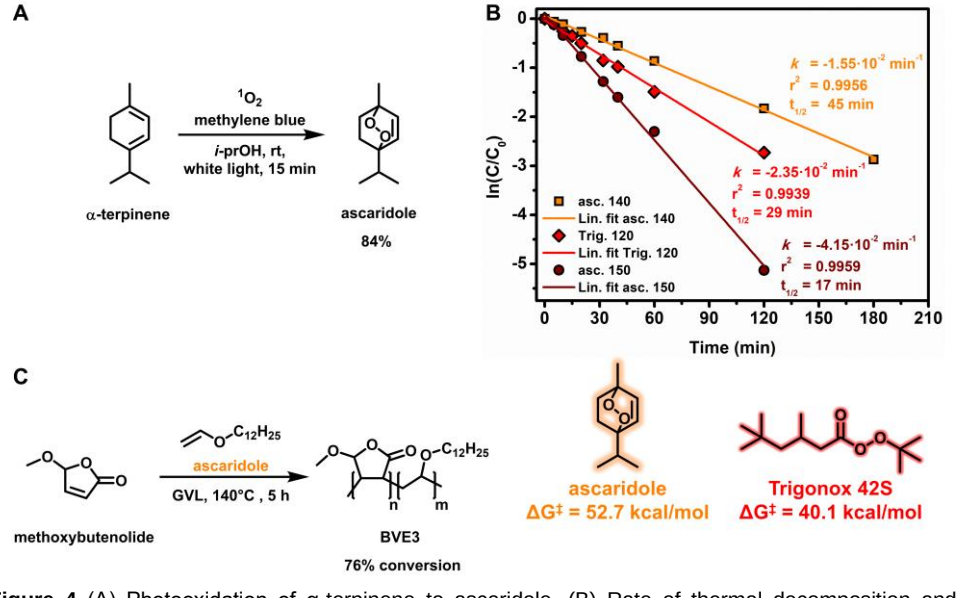

Figure 4 (A) Photooxidation of α-terpinene to ascaridole. (B) Rate of thermal decomposition and determination of the half-life time of ascaridole at 140°C (orange squares), 150°C (brown circles) and Trigonox 42S at 120°C (red diamonds) monitored by ^{1}H-NMR spectroscopy by taking samples at regular intervals (top) and computationally calculated energies of radical initiators (bottom). Reaction conditions: radical initiator 0.5 M, GVL, 3 h. (C) Copolymerization of methoxybutenolide and dodecyl vinyl ether using ascaridole (6 mol%) as radical initiator.

Performing the copolymerization of methoxybutenolide and dodecyl vinyl ether in GVL at 140°C using ascaridole (6 mol%) resulted in 76% conversion after 5 h, clearly demonstrating the viability of ascaridole as a fully biobased thermal radical initiator for the free radical polymerization of fully biobased components (**Figure 4C**). Following the reaction kinetics of the copolymerization, incorporation of both monomers was confirmed, albeit with a slightly diminished amount of methoxybutenolide. Furthermore, the copolymerization shows an initial fast conversion with a rate constant (k_{obs}) in the same order of magnitude as determined for the copolymerization in butyl acetate, followed by a slower conversion (see **Experimental Section Figure S12**). Performing the copolymerization at 150°C did not meaningfully impact the polymerization behavior.

Focusing on the polymer properties, the molecular weights for the copolymers synthesized with ascaridole in GVL and with Trigonox 42S in butyl acetate and GVL were analyzed and summarized in **Table 2**. A higher rate constant is observed upon changing the solvent from butyl acetate to GVL, attributing to a higher observed molecular weight. We propose there is an increased compatibility of the reacting monomers with the more polar solvent GVL.

Substituting Trigonox 42S with fully biobased ascaridole as the radical initiator results in a lower molecular weight being observed, in line with the incomplete conversion and the lower rate of polymerization, which indicates termination reactions to be involved at a larger extent (**Table 2**).

Table 2 Polymer properties of methoxybutenolide-dodecyl vinyl ether copolymers. **BVE1** = copolymer synthesized in butyl acetate at 120°C using Trigonox 42S as radical initiator, **BVE2** = copolymer synthesized in GVL at 120°C using Trigonox 42S as radical initiator. **BVE3** = copolymer synthesized in GVL at 140°C using ascaridole as radical initiator.

Copolymers[a]	k_{obs} (s^{-1})	Conversion (%)	M_n (kDa)	M_w (kDa)	D[b]
BVE1	$6.10 \cdot 10^{-4}$	95	1.3	2.9	2.2
BVE2	$1.15 \cdot 10^{-3}$	>99	2.0	3.6	1.7
BVE3	$3.23 \cdot 10^{-4}$	76	1.0	2.0	2.0

[a]Reaction conditions: 1:1 ratio of monomers, thermal initiator (6 mol%), 2 M in solvent at given T, 2–5 h. [b]Polydispersity (D) is calculated by dividing M_w by M_n.

3.2.4 Coating formation

Having established that full biobased polymers could be formed using ascaridole as thermal initiator in combination with two biobased monomers, we proceeded to the formation of surface coatings. Previously we have shown excellent hard transparent coatings could be formed through solvent-free UV-curing using alkoxybutenolides in combination with a divinyl ether based crosslinker and a phosphine oxide photoinitiator.[26] Utilizing the described robust sustainable vinylation method, a biobased divinyl ether crosslinker (1,4-butane divinyl ether) was undemandingly prepared from the glucose-derived 1,4-butanediol.[33] The final remaining component of the coating mixture to be made from biorenewable resources is the photoinitiator. Recently, Versace *et al.* described the synthesis of a vanillin-based type I photoinitiator (**Figure 5A**).[57] We envisioned that the biobased photoinitiator, **VAPO**, could be a direct replacement of the previously used **BAPO** photoinitiator, as they both contain a similar acyl-phosphine oxide structure and exert similar reactivity. **VAPO** was thus synthesized according to a literature procedure in a three-step process from vanillin *via* allylation, tertiary phosphine oxide formation and alcohol oxidation with high yields (**Figure 5A**). The UV-Vis absorption spectrum of **VAPO** revealed, although a slightly lower intensity of absorption at λ = 395 nm compared to **BAPO**, that the photoinitiator is suitable for the comonomers and our current UV-curing setup (**Figure 5B**). A homogeneous neat mixture of methoxybutenolide (1 eq.), 1,4-butane divinyl ether (0.5 eq.) and **VAPO** (6 mol%) was applied on a 20 x10 cm glass panel and irradiated for 20 min using a UV-Flood lamp 36 (35 W) UVA lamp (**Figure 5C**). A clear, hard, transparent and above all biobased coating of 50 µm was obtained on glass. Lower loading of **VAPO** (3 mol%) resulted in a tacky coating, justifying the higher loading of **VAPO** (6 mol%) (**Experimental Section Figure S13** and **Figure S14**). Interestingly, applying 3 mol% of the original photoinitiator **BAPO** together with the methoxybutenolide (1 eq.) and 1,4-butane divinyl ether (0.5 eq.) resulted in a hard but semi-clear coating, presumably caused by unreacted monomers (**Experimental Section Figure S13** and **Figure S14**).

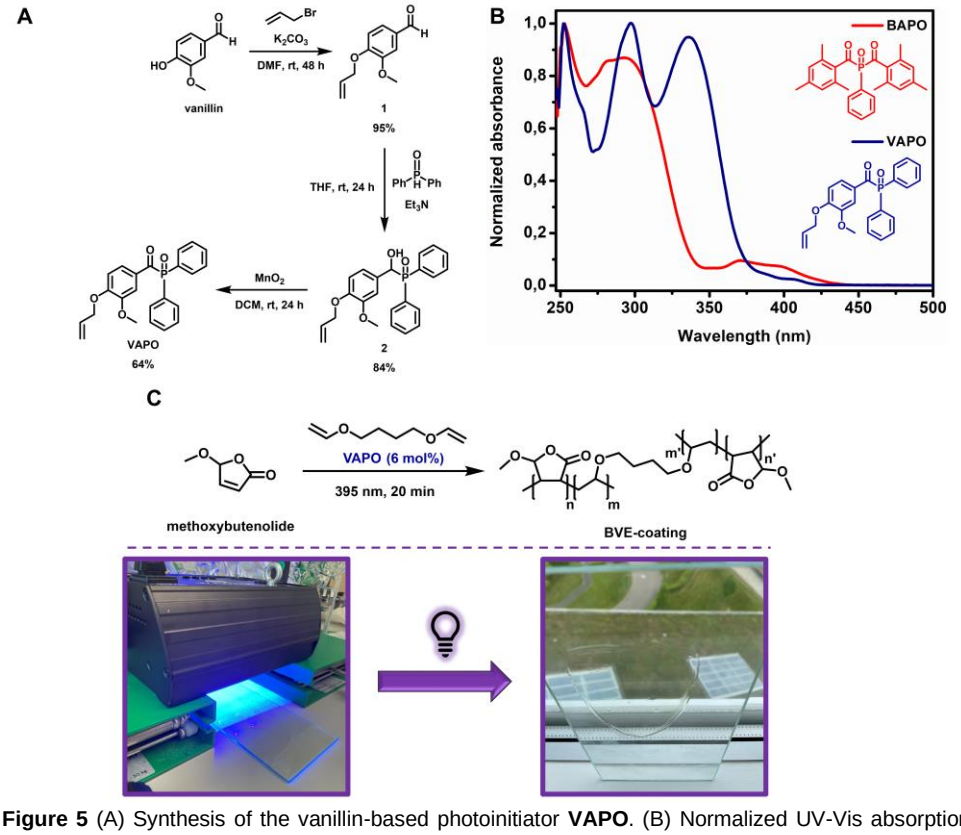

Figure 5 (A) Synthesis of the vanillin-based photoinitiator **VAPO**. (B) Normalized UV-Vis absorption spectra of the previously used **BAPO** (red) and the biobased **VAPO** (navy). (C) Crosslinking of alkoxybutenolides (1 eq.) with 1,4-butane divinyl ether (0.5 eq.), **VAPO** (6 mol%) as radical initiator and UV light (λ_{irr} = 395 nm, 20 min) as trigger (top), UV-curing of coating mixture on glass panel (bottom).

To determine the properties of the **VAPO**- and **BAPO**-initiated biobased coatings, we subjected the materials to a Knoop hardness test and Differential Scanning Calorimetry (DSC) to establish the hardness and the glass transition temperature (T_g), respectively. Both coatings display similar properties, showing effective replacement of **BAPO** with the vanillin-based **VAPO** (**Table 3**). Values found for the hardness and the T_g are typically in the range of hard acrylate based coatings.[58, 59] Furthermore the coatings were subjected to a 2-butanone (MEK) double rub test where excellent solvent resistance (>200 double rubs) was observed with no deterioration of the surface except for slight whitening (**Experimental Section Figure S15**).

Table 3 Summary of methoxybutenolide – 1,4-butane divinyl ether coatings on glass. Coating formation conditions: methoxybutenolide (1 eq.), 1,4-butane divinyl ether (0.5 eq.), photoinitiator (3 mol%), UV light (λ_{irr} = 395 nm), 20 min.

Coatings	Initiator	Dry film Thickness (µm)	Knoop hardness (kg/mm^2)	T_g (°C)	MEK resistance (double rubs)
BVEC1	**VAPO**[a]	50	9.9 (± 0.1)	24	>200
BVEC2	**BAPO**	55	13.9 (± 4.3)	43	>200

[a]6 mol% initiator for formation of uniform tacky-free coating.

3.3 Conclusion

In conclusion, we have developed a polymer and coating system using starting materials derived from renewable resources and implementing sustainable synthetic steps. The main monomers used in the polymerization were synthesized from the platform chemical furfural and common biobased alcohols, using molecular oxygen (in a photosensitization process) and calcium carbide as sustainable reagents. The biobased photosensitizer **FLY 450**, used in the photooxidation of furfural, showed excellent photosensitization properties with high molar extinction coefficients and quantum yields. The biobased methoxybutenolide–dodecyl vinyl ether copolymer was synthesized in high conversion in the green solvent GVL using the natural oil-derived radical initiator ascaridole, resulting in a fully biobased and sustainable polymer. Finally a fully biobased coating was formed using a vanillin derived photoinitiator on a glass surface which exhibits excellent hardness and outstanding solvent resistance in line with properties of hard acrylate based coatings. This integrated sustainable polymer and coating system illustrates viable and promising green alternatives for key components used in the production of materials widely abundant in modern society.

3.4 Author Contributions

Ben Feringa conceptualized the research project and coordinated it with the help of Keimpe van den Berg. George Hermens and Thomas Freese synthesized the biobased components. George Hermens and Mathieu Lepage synthesized the polymers, performed kinetics experiments and measured the polymer properties. George Hermens carried out the coating formation. Georgios Alachouzos performed the DFT studies. Niels Elders determined the coating properties.

3.5 Acknowledgements

We thank Oetze Staal for technical support regarding the photooxidation setups, Renze Sneep, and Johan Hekelaar for assistance with HRMS.

3.6 Experimental Section

For the general methods section, please refer to **Appendix, General Information**. Photooxidation reactions were performed in dedicated setups described in **Figure S3** and **Figure S4**. Unless stated otherwise alle reactions were carried out under a nitrogen atmosphere using Schlenk and vacuum-line techniques. Polymerization reactions were performed in a 4 mL glass vial with screw cap and septum. Coating formation experiments were performed on glass plates (10 x 20 cm).

3.6.1 DFT calculations

All computational input files were prepared in GaussView 6.0 on a local Windows 10 terminal. Input files were then transferred to the Rijksuniversiteit Groningen Peregrine HPC cluster where DFT or TD-DFT calculations were carried out using the Gaussian 16 (g16) suite of programs.

The DFT or TD-DFT energies for the S_0 ground state and both S_1 and T_1 excited states of **FLY 450**, were obtained at the MN15/Def2TZVPP/SMD=MeOH and the MN15/Def2TZVPP/SMD=DCM level. Geometry optimization to the most stable double bond isomer of either ground state S_0 or excited state S_1 or T_1 minima was carried out using the g16 *opt* command at the MN15 functional and Def2TZVPP basis set level of theory with implicit solvation using the Solvation Model based on Density (SMD = MeOH or DCM),[37-39] and the energies reported were read from the g16 output file. Vertical excitations are obtained from a TD-DFT calculation at the MN15/Def2TZVPP/SMD=MeOH and the MN15/Def2TZVPP/SMD=DCM level, using the S_0 geometry optimized at the same level of theory as the input geometry.

Table S1 The computed excited state S1 or T1 and vertical excitation energies of **FLY 450**.

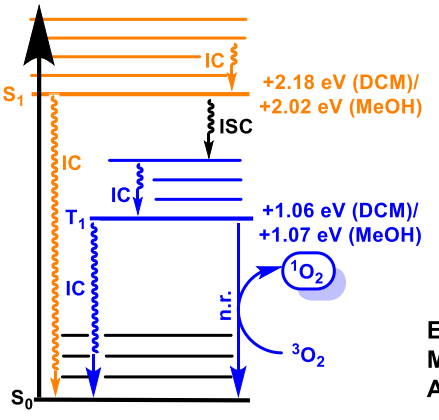

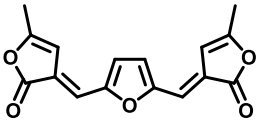

FLY 450

*excitation** +2.64 eV (DCM)/ +2.62 eV (MeOH)

(+2.76 eV from experiment)

S_1-T_1 energy gap: 1.12 eV (DCM) 1.05 eV (MeOH)

Energies of structures optimized at the MN15/Def2TZVPP/SMD=MeOH or DCM level. All values in eV.

	MN15/Def2TZVPP/SMD=DCM	MN15/Def2TZVPP/SMD=MeOH
predicted λ_{max}	470 nm	473 nm
singlet S_1 state	+2.18 eV	+2.02 eV
triplet T_1 state	+1.06 eV	+1.07 eV
S_1-T_1 energy gap	**1.12 eV**	**1.05 eV**

The DFT thermochemistry of decomposition pathways for **FLY 450** - endoperoxide in MeOH was also calculated. Stationary points, in addition to transition states leading to two proposed decomposition products were examined at the MN15/Def2TZVPP/SMD=MeOH level. Geometry optimization to either stationary point structures or transition state (TS) structures were carried out using the g16 *opt* command at the MN15 functional and Def2SVP basis set level of theory with implicit solvation using the Solvation Model based on Density (SMD = MeOH).[37-39] Transition state geometry inputs were the result of rational guess based on bond length during bond breaking or forming events, or were the result of potential energy surface relaxed coordinate scans using the g16 *scan* command at the MN15/Def2SVP/SMD=MeOH level. Intrinsic reaction coordinate (IRC)iv calculations were carried out on the transition state structures to verify that they connected to the associated reactant and product minima structures. After optimization, frequency DFT calculations of all obtained optimized structures were carried out using the g16 *freq* command at the MN15/Def2TZVPP/SMD=MeOH level, to confirm that minima structures had zero imaginary frequencies and that transition states had a single imaginary frequency. All shown free energies (**Figure S1**) are ZPE and thermally corrected and were obtained from the frequency calculations. All shown free energies are reported in kcal/mol, at 298.15 K / 1 atm.

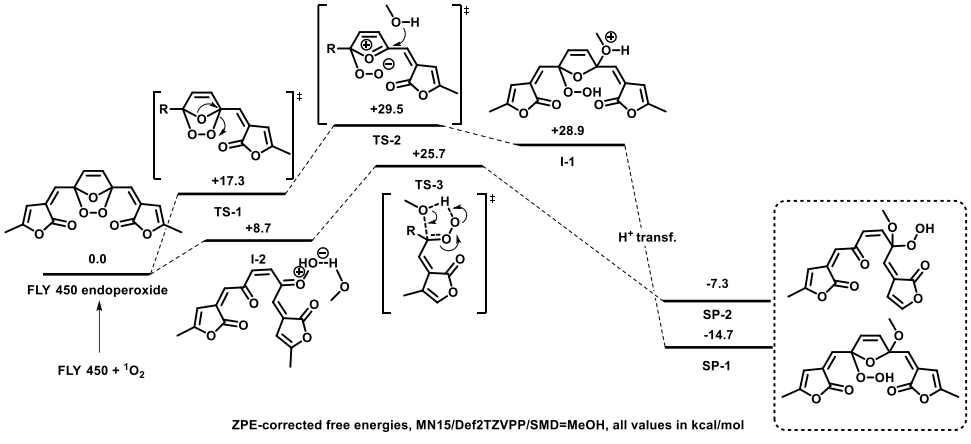

Figure S1 The computed free energies for the decomposition pathway of the FLY 450 endoperoxide.

The DFT thermochemistry of the homolytic *O-O bond* scission for both ascaridole and Trigonox 42s (acetate used instead of 3,5,5-trimethylhexanoate) was calculated. A reactant stationary point, in addition to the homolytic *O-O bond* scission transition state was examined at the MN15/Def2TZVPP/SMD=THF level, as THF from the g16 package has the closest polarity to the employed gamma-valerolactone (GVL). Geometry optimization to either stationary point structures or transition state (TS) structures were carried out using the g16 *opt* command at the MN15 functional and Def2TZVPP basis set level of theory with implicit solvation using the Solvation Model based on Density (SMD = THF).[37-39] Transition state geometry inputs were the result of potential energy surface relaxed coordinate scans using the g16 *scan* command at the MN15/Def2TZVPP/SMD=THF level. Intrinsic reaction coordinate (IRC)iv calculations were carried out on the transition state structures to verify that they connected to the associated reactant and product minima structures. After optimization, frequency DFT calculations of all obtained optimized structures were carried out using the g16 *freq* command at the MN15/Def2TZVPP/SMD=THF level, to confirm that minima structures had zero imaginary frequencies and that transition states had a single imaginary frequency. All shown free energies (**Figure S2**) are ZPE and thermally corrected and were obtained from the frequency calculations. All shown free energies are reported in kcal/mol, at 298.15 K / 1 atm.

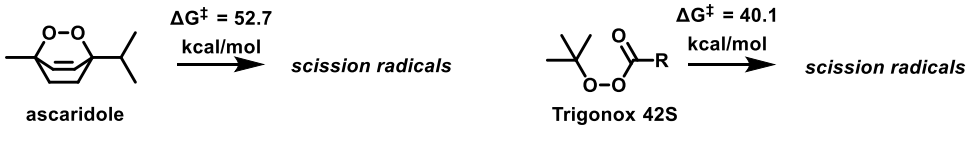

Figure S2 The computed barrier of activation for the homolytic decomposition of biobased radical initiator ascaridole and reference radical initiator Trigonox 42S.

3.6.2 Compound preparation and characterization

FLY 450

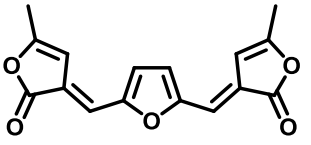

A solution of diformylfuran (100 mg, 0.81 mmol, 1 eq.), α-angelica lactone (237 mg, 2.42 mmol, 3 eq.) and $CaCO_3$ (242 mg, 2.42 mmol, 3 eq.) in demineralized H_2O (5.5 mL, 0.15 M) was prepared and stirred at reflux for 3 h. The reaction mixture was allowed to cool down, subsequently filtered and the volatiles were removed under reduced pressure. The residue was dissolved in EtOAc (10 mL), activated charcoal (500 mg) was added and the suspension was stirred at room temperature for 1 h. The mixture was filtered and concentrated under reduced pressure to obtain **FLY 450** as a bright red solid (160 mg, 0.56 mmol, 70%).

^{1}H NMR (400 MHz, $CDCl_3$) δ 6.97 (t, *J* = 0.9 Hz, 2H), 6.83 (s, 2H), 6.42 (t, *J* = 1.3 Hz, 2H), 2.25 (t, *J* = 1.1 Hz, 6H).

^{13}C NMR (101 MHz, $CDCl_3$) δ 159.1, 154.8, 124.7, 120.1, 117.6, 104.0, 15.5.

HRMS calculated 286.07910, found 286.07896.

Hydroxybutenolide (rotary photoreactor, methylene blue as photosensitizer)

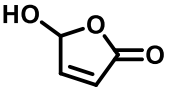

A solution of freshly distilled (50°C, 1x10^{-2} mbar) furfural (1.0 g, 10 mmol, 1 eq.) and methylene blue (17 mg, 52 µmol, 0.5 mol%) in 10 mL O_2 enriched methanol (1 M) was prepared in a round bottom flask (1 L). The mixture was put under an O_2 atmosphere in a standard lab rotary evaporator (175 rpm), as described *vide infra*, and irradiated by 10 LED lamps (8 W per LED, 80 W total) at room temperature for 20 min. The light sources were placed at a distance of approximately 5 cm from the flask. After the reaction, methanol was evaporated under reduced pressure. The obtained oil solidified upon standing. The product 5-hydroxy-2(5H)-furanone could be used without further purification (1.0 g, 10 mmol, >99% yield). A detailed purification method is described in the **Experimental Section (5.6.4)** of **Chapter 5**.

^{1}H NMR (400 MHz, $CDCl_3$) δ 7.31 (d, J = 5.7 Hz, 1H), 6.25 (s, 1H), 6.23 (d, J = 5.7 Hz, 1H), 5.04 (s, 1H).

^{13}C NMR (101 MHz, $CDCl_3$) δ 171.8, 152.3, 124.7, 99.1.

HRMS calculated 99.0088, found 99.0090.

Hydroxybutenolide (batch photooxygenation, FLY 450 as photosensitizer)

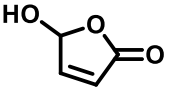

A solution of freshly distilled (50°C, 1x10^{-2} mbar) furfural (35 mg, 362 µmol, 1 eq.) and **FLY 450** (1 mg, 3.5 µmol, 1 mol%) in 5 mL O_2 enriched methanol (0.1 M) was prepared in a 5 mL vial with septum. The mixture was irradiated at room temperature with blue light (LED, 500 mW, λ = 445 nm, 180 mW/cm^2), as described *vide infra* for 20 h. After the reaction, methanol was evaporated under reduced pressure. The obtained oil solidified upon standing. The product 5-hydroxy-2(5H)-furanone could be used without further purification (36 mg, 362 mmol, >99% yield).

^{1}H NMR (400 MHz, $CDCl_3$) δ 7.31 (d, J = 5.7 Hz, 1H), 6.25 (s, 1H), 6.23 (d, J = 5.7 Hz, 1H), 5.04 (s, 1H).
^{13}C NMR (101 MHz, $CDCl_3$) δ 171.8, 152.3, 124.7, 99.1.
HRMS calculated 99.0088, found 99.0090.

Ascaridole (rotary photoreactor, methylene blue as photosensitizer)

A solution of α-terpinene (250 mg, 1.84 mmol, 1 eq.) and methylene blue (12 mg, 37 µmol, 2 mol%) in 10 mL O_2 enriched *i*-PrOH (0.18 M) was prepared in a round bottom flask (1 L). The mixture was put under an O_2 atmosphere in a standard lab rotary evaporator (175 rpm), as described *vide infra*, and irradiated by 10 LED lamps (8 W per LED, 80 W total) at room temperature for 20 min. The light sources were placed at a distance of approximately 5 cm from the flask. After the reaction, *i*-PrOH was carefully evaporated under reduced pressure and an oil was obtained. The oil was further purified by column chromatography (silica gel, n-pentane/ethyl acetate : 90/10, R_f = 0.5), yielding ascaridole (260 mg, 1.55 mmol, 84%) as a slightly yellow oil.
^{1}H NMR (400 MHz, $CDCl_3$) δ 6.49 (d, *J* = 8.5 Hz, 1H), 6.40 (d, *J* = 8.5 Hz, 1H), 2.10 – 1.95 (m, 2H), 1.91 (dq, *J* = 13.9, 6.8 Hz, 1H), 1.64 – 1.46 (m, 2H), 1.37 (s, 3H), 0.99 (d, *J* = 7.0 Hz, 6H).
^{13}C NMR (101 MHz, $CDCl_3$) δ 136.5, 133.2, 79.9, 74.5, 32.3, 29.6, 25.7, 21.5, 17.4, 17.3.
HRMS calculated 170.12566, found 170.12560.

Methoxybutenolide

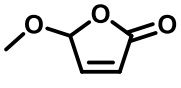

Hydroxybutenolide (10 g, 100 mmol) was dissolved in 100 ml methanol and heated at reflux for 20 hours. The conversion was followed by ^{1}H NMR until all hydroxybutenolide was consumed. The solvent was evaporated under reduced pressure, and the crude was distilled under reduced pressure (70°C, 1.0 × 10^{-2} mbar), yielding methoxybutenolide (8.7 g, 76 mmol, 76%) as a slightly yellow oil.
^{1}H NMR (400 MHz, $CDCl_3$) δ 7.20 (dd, J = 5.7, 1.2 Hz, 1H), 6.24 (dd, J = 5.7, 1.2 Hz, 1H), 5.86 (t, J = 1.2 Hz, 1H), 3.58 (s, 3H).
^{13}C NMR (101 MHz, $CDCl_3$) δ 193.9, 150.2, 125.4, 104.2, 57.2.
HRMS calculated 115.03897, found 115.038892.

Dodecyl vinyl ether

A solution of dodecanol (500 mg, 2.68 mmol 1 eq.), KOH (166 mg, 2.95 mmol, 1.1 eq.), KF (624 mg, 10.73 mmol, 4 eq.) and calcium carbide (1.03 g, 16.10 mmol, 6 eq.) in 13 mL DMSO (0.2 M) was prepared according to the literature procedure[53] and added to a pressure flask. H_2O (1.2 mL, 24 eq., 4:1 calcium carbide) was added and the pressure flask was sealed tight. The reaction mixture was heated to 130°C and stirred for 3 h. After completion, the reaction mixture was extracted with hexane (3 x 20 mL) and the crude solution was filtered over celite. The solvent was

evaporated under reduced pressure and the resulting oil was further purified by column chromatography (silica gel, n-pentane, R_f = 0.7) to obtain dodecyl vinyl ether (416 mg, 1.96 mmol, 73%) as a colorless oil.
^{1}H NMR (400 MHz, $CDCl_3$) δ 6.47 (ddd, *J* = 14.4, 6.8, 1.6 Hz, 1H), 4.17 (dt, *J* = 14.3, 1.8 Hz, 1H), 3.97 (dt, *J* = 6.8, 1.8 Hz, 1H), 1.71 – 1.59 (m, 2H), 1.45 – 1.15 (m, 21H), 0.88 (td, *J* = 6.9, 1.7 Hz, 7H).
^{13}C NMR (101 MHz, $CDCl_3$) δ 152.2, 86.3, 68.3, 32.1, 29.8, 29.8, 29.7, 29.7, 29.5, 29.5, 29.2, 26.2, 22.8, 14.3.

1,4-butanedivinyl ether

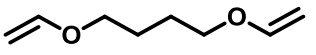

A solution of 1,4-butanediol (500 mg, 5.55 mmol 1 eq.), KOH (685 mg, 12.21 mmol, 2.2 eq.), KF (2.58 g, 44.38 mmol, 8 eq.) and calcium carbide (4.27 g, 66.58 mmol, 12 eq.) in 28 mL DMSO (0.2 M) was prepared according to the literature procedure[53] and added to a pressure flask. H_2O (4.8 mL, 48 eq., 4:1 calcium carbide) was added and the pressure flask was sealed tight. The reaction mixture was heated to 130°C and stirred for 3 h. After completion, the reaction mixture was extracted with hexane (3 x 40 mL) and the crude solution was filtered over celite. The solvent was evaporated under reduced pressure and the resulting oil was further purified by column chromatography (silica gel, n-pentane, R_f = 0.7) to obtain 1,4-butanedivinyl ether as a colorless oil (550 mg, 3.87 mmol, 70%).
^{1}H NMR (400 MHz, $CDCl_3$) δ 6.46 (dd, *J* = 14.3, 6.8 Hz, 1H), 4.17 (dd, *J* = 14.3, 2.0 Hz, 1H), 3.98 (ddd, *J* = 6.8, 2.0, 0.7 Hz, 1H), 3.71 (h, *J* = 3.1 Hz, 2H), 1.76 (tt, *J* = 3.5, 1.8 Hz, 2H).
^{13}C NMR (101 MHz, $CDCl_3$) δ 152.0, 86.5, 67.7, 25.9.
HRMS calculated 143.10666, found 143.10664.

4-(allyloxy)-3-methoxybenzaldehyde (1)

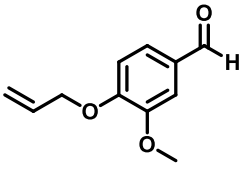

A solution of vanillin (5.0 g, 32.86, 1 eq.) in DMF (66 mL, 0.5 M) was prepared and cooled to 0°C. K_2CO_3 (18.17 g, 131.45 mmol, 4 eq.), was added and the solution was stirred for 10 min. Allyl bromide (15.9 g, 131.45 mmol, 4 eq.) was added over 30 min and the reaction mixture was allowed to warm up to room temperature. The mixture was stirred for 24 h at room temperature in which full conversion was achieved. Demineralized water (150 mL) was added and the reaction mixture was extracted with ethyl acetate (3 x 150 mL). The organic phase was washed 7 times with demineralized water (150 mL) to remove residual DMF. The organic phase was dried with $MgSO_4$, filtered and the solvent, unreacted allyl bromide and allyl alcohol were evaporated under reduced pressure (60°C, 1 mbar) to obtain 4-(allyloxy)-3-methoxybenzaldehyde as a yellow viscous oil (6.0 g, 31.22 mmol, 95%).
^{1}H NMR (400 MHz, $CDCl_3$) δ 9.84 (d, *J* = 1.9 Hz, 1H), 7.42 (dd, *J* = 7.0, 1.9 Hz, 2H), 6.97 (dd, *J* = 8.8, 1.9 Hz, 1H), 6.07 (dddd, *J* = 17.8, 10.7, 5.4, 2.8 Hz, 1H),

5.43 (dp, *J* = 17.3, 1.6 Hz, 1H), 5.33 (dt, *J* = 10.5, 1.7 Hz, 1H), 4.70 (dq, *J* = 5.3, 1.7 Hz, 2H), 3.93 (d, *J* = 1.9 Hz, 3H).
^{13}C NMR (101 MHz, $CDCl_3$) δ 190.7, 153.3, 149.7, 132.0, 130.9, 126.4, 118.6, 111.7, 109.1, 69.6, 55.8.
HRMS calculated 193.08592, found 193.08580.

((4-(allyloxy)-3-methoxyphenyl)(hydroxy)methyl)diphenylphosphine oxide (2)

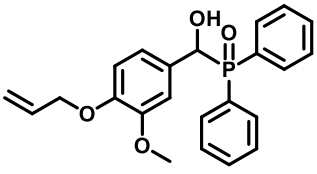

A solution of 4-(allyloxy)-3-methoxybenzaldehyde (2.0 g, 10.41 mmol, 1 eq.) and diphenylphosphine oxide (2.10 g, 10.41 mmol, 1 eq.) in anhydrous THF (40 mL, 0.26 M) was prepared and stirred at room temperature. Anhydrous triethylamine (1.05 g, 1.4 mL, 10.41 mmol, 1 eq.) was added dropwise and reaction mixture was stirred for 24 h, in which a white precipitate was formed. The precipitated produced was filtered, washed with cold THF and dried in air to obtain ((4-(allyloxy)-3-methoxyphenyl)(hydroxy)methyl)diphenylphosphine oxide as a white solid (3.45 g, 8.75 mmol, 84%).
^{1}H NMR (400 MHz, $CDCl_3$) δ 7.75 (ddt, *J* = 10.9, 8.2, 1.3 Hz, 1H), 7.58 – 7.31 (m, 3H), 6.72 – 6.63 (m, 1H), 6.59 (s, 1H), 6.04 (ddtd, *J* = 17.1, 10.7, 5.4, 1.2 Hz, 0H), 5.43 – 5.30 (m, 1H), 5.26 (dq, *J* = 10.5, 1.4 Hz, 0H), 4.63 (s, 0H), 4.57 – 4.49 (m, 1H), 3.53 (d, *J* = 1.2 Hz, 2H).
^{13}C NMR (101 MHz, $CDCl_3$) δ 148.7, 147.6, 133.0, 132.3, 132.2, 132.0, 131.9, 131.7, 128.2, 128.1, 128.0, 128.0, 120.0, 117.8, 112.5, 110.7, 74.2, 73.3, 55.4.
^{31}P NMR (162 MHz, $CDCl_3$) δ 30.59.
HRMS calculated 395.14067, found 395.14042.

(4-(allyloxy)-3-methoxyphenyl)(diphenylphosphoryl)methanone (VAPO)

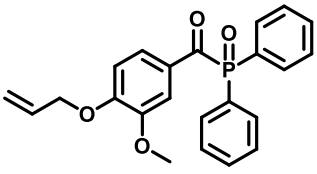

A solution of ((4-(allyloxy)-3-methoxyphenyl)(hydroxy)methyl)diphenylphosphine oxide (1.0 g, 2.54 mmol, 1 eq.) in anhydrous DCM (25 mL, 0.1 M) was prepared and stirred at room temperature. Activated MnO_2 (4.41 g, 50.71 mmol, 20 eq.) was added and the reaction mixture was purged with N_2 for 30 min. Thereafter, the reaction mixture was stirred at room temperature for 24 hours. The solution was filtered over celite and protected from light. The solvent was evaporated under reduced pressure and the resulting crude solid was further purified by column chromatography (silica gel, n-pentane/ethyl acetate : 90/10, R_f = 0.5) to obtain (4-(allyloxy)-3-methoxyphenyl)(diphenylphosphoryl)methanone (**VAPO**) as a white solid (0.64 g, 1.63 mmol, 64%).
^{1}H NMR (400 MHz, $CDCl_3$) δ 8.56 (dd, *J* = 8.6, 1.9 Hz, 1H), 7.92 – 7.81 (m, 5H), 7.59 – 7.44 (m, 6H), 6.91 (d, *J* = 8.6 Hz, 1H), 6.05 (ddt, *J* = 16.5, 10.7, 5.4 Hz, 1H), 5.42 (dd, *J* = 17.4, 6.7 Hz, 1H), 5.32 (d, *J* = 10.4 Hz, 1H), 4.69 (d, *J* = 5.5 Hz, 2H), 3.91 (d, *J* = 11.3 Hz, 3H).

^{13}C NMR (101 MHz, $CDCl_3$) δ 132.6, 132.5, 132.5, 132.2, 132.1, 132.0, 128.8, 128.7, 127.3, 124.4, 119.1, 118.8, 112.8, 112.1, 112.0, 111.0, 111.0, 70.9, 56.1.
^{31}P NMR (162 MHz, $CDCl_3$) δ 22.28.
HRMS calculated 393.12502, found 393.12474.

Copolymerization methoxybutenolide and dodecyl vinyl ether (BVE1, BVE2) (Trigonox 42S)

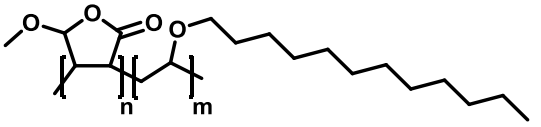

To a 4-ml vial with screwcap with septum, a solution of methoxybutenolide (100 mg, 0.88 mmol, 1 eq.) and dodecyl vinyl ether (186 mg, 0.88 mmol, 1 eq.) in butyl acetate or GVL (0.44 ml) were added. The mixture was heated to 120°C, and Trigonox 42S (12 mg, 0.013 µl, 0.05 mmol, 0.06 eq.) was added to initiate polymerization. The mixture was refluxed for 2 h. The reaction mixture was concentrated under reduced pressure to obtain the methoxybutenolide-dodecyl vinyl ether copolymers, **BVE1** (butyl acetate), **BVE2** (GVL) with 95% and >99% conversion, respectively.

1,3,5-Trimethoxybenzene (49 mg, 0.29 mmol, 0.33 eq.) was added as an internal standard before the initiation for ^{1}H NMR kinetic measurements. At regular intervals, a sample of 50 µL was taken from the mixture and put in a small vial, which was flash frozen (−18°C) to stop polymerization.

Copolymerization methoxybutenolide and dodecyl vinyl ether (BVE3) (ascaridole)

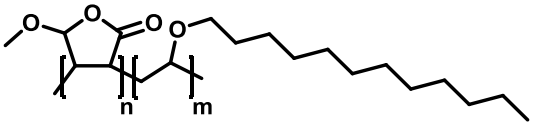

To a 4-ml vial with screwcap with septum, a solution of methoxybutenolide (100 mg, 0.88 mmol, 1 eq.) and dodecyl vinyl ether (186 mg, 0.88 mmol, 1 eq.) in GVL (0.44 ml) were added. The mixture was heated to 140°C, and ascaridole (9 mg, 0.05 mmol, 0.06 eq.) was added to initiate polymerization. The mixture was refluxed for 5 h. The reaction mixture was concentrated under reduced pressure to obtain the methoxybutenolide-dodecyl vinyl ether copolymer, **BVE3** with 76% conversion.

1,3,5-Trimethoxybenzene (49 mg, 0.29 mmol, 0.33 eq.) was added as an internal standard before the initiation for ^{1}H NMR kinetic measurements. At regular intervals, a sample of 50 µL was taken from the mixture and put in a small vial, which was flash frozen (−18°C) to stop polymerization.

UV curing of butenolide based coatings

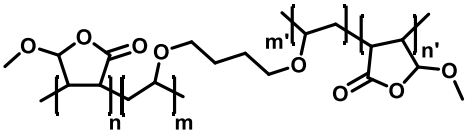

To a 4 ml vial, methoxybutenolide (200 mg, 1.75 mmol, 1 eq.), 1,4-butanedivinyl ether (125 mg, 0.88 mmol, 0.5 eq.), and phenylbis(2,4,6-trimethylbenzoyl)phosphine oxide (**BAPO**) (22 mg, 53 µmol, 3 mol%) or (4-(allyloxy)-3-methoxyphenyl)(diphenylphosphoryl)methanone (**VAPO**) (41 mg, 105 µmol, 6 mol%) were added and stirred until the reaction mixture became homogeneous. The mixture was applied on a glass surface, and the surface (10 × 20 cm) was coated with a Byk applicator (50 µm thickness). The glass surface was irradiated with λ = 395 nm light (UV Flood 36, 12 x 3 W) at 5-cm distance for 20 min.

3.6.3 Photooxygenation setups

Photovap (rotary evaporator)

The previously described rotary evaporator allows for efficient larger scale photooxygenation due the fast rotation creating a thin film, optimal for light penetration, and creating a high mass transfer of oxygen into the solution. To allow for an oxygen atmosphere in the rotary photoreactor, the photoreactor was purged with O_2 through vacuum/oxygen cycles using an O_2 filled balloon that was attached to the rotary evaporator. A home-built white light setup (575 lm, 8 W each; 5750 lm, 80 W total) consisting of standard white light LED bulbs was placed at a distance of approximately 5 cm around the 1 L flask, containing the reaction mixture (**Figure S3**). The photooxygenations were carried out according to the **Compound preparation and characterization**.

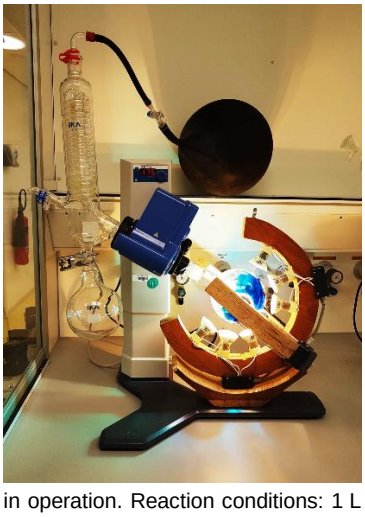

Figure S3 Rotary photoreactor in operation. Reaction conditions: 1 L flask, 1 M furfural in MeOH (10 mL),10 x 8W LED, 0.5 mol% methylene blue.

Batch photooxygenation

The previously described rotary evaporator was used for the preliminary experiment utilizing **FLY-450** (0.5 mol%) as photosensitizer. Photooxidation of furfural (1.0 g, 10 mmol, 1 eq.) led to 85% conversion towards hydroxybutenolide in 1h (**Figure S4**, left).

The smaller scale photooxygenation using **FLY 450** as photosensitizer was carried out in 5 mL vial, in a block of 6 slots, with irradiation of 500 mW LED from the bottom (**Figure S4**, right). To allow for an oxygen atmosphere and saturation of the solution, oxygen was bubbled using a needle. The temperature of the LEDs was controlled at 20°C by a liquid circulator. The photooxygenation was carried out according to the **Compound preparation and characterization.**

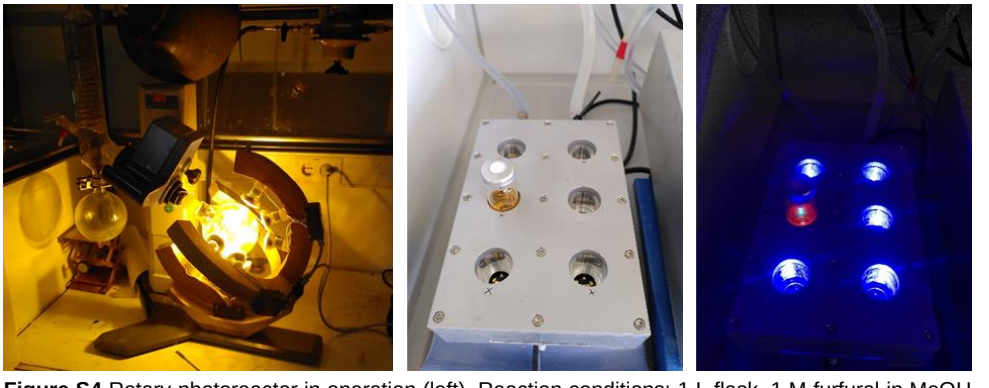

Figure S4 Rotary photoreactor in operation (left). Reaction conditions: 1 L flask, 1 M furfural in MeOH (10 mL),10 x 8W LED, 0.5 mol% FLY 450. Batch photooxygenation in operation (middle/right). Reaction conditions: 5 mL vial with septum, 0.07 M furfural in MeOH (5 mL),1 x 500 mW LED (λ_{irr} = 445 nm), 1 mol% FLY 450.

3.6.4 Normalized UV VIS absorption spectrum

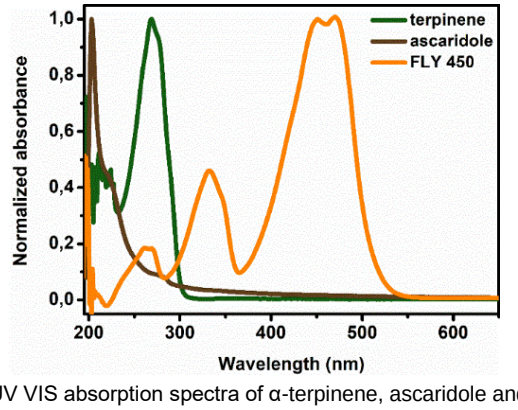

Figure S5 Normalized UV VIS absorption spectra of α-terpinene, ascaridole and **FLY 450**.

3.6.5 Normalized emission spectra

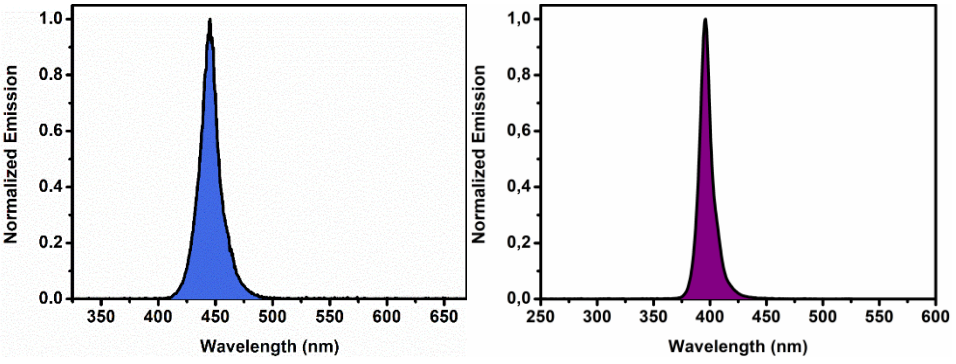

Figure S6 Normalized emission spectrum LED OSRAM Oslon SSL 80 royal blue (500 mW, λ = 445 nm, 180 mW/cm^2) as light source for batch photooxygenations (left) and normalized emission spectrum LED Beacon UV FLOOD 395 nm (12 x 3 W, λ = 395 nm, 21 mW/cm^2) for coating formation (right).

3.6.6 Singlet oxygen quantum yield

In order to determine the quantum yield of **FLY 450** in methanol and dichloromethane the scavenger decay rate was determined. Originally, 1,3-Diphenylisobenzofuran (DPiBF) was used (λ_{max} = 450 nm). However using blue light irradiation DPiBF showed undesired self-photosensitization towards singlet oxygen at 445 nm.[60] Therefore it was decided to utilize the biobased singlet oxygen scavenger α-terpinene. (**Figure S7**).

As **FLY 450** contains a similar furan moiety as DPiBF and furfural, slight photobleaching was observed in MeOH, which was also confirmed by DFT studies (**Figure S1**).

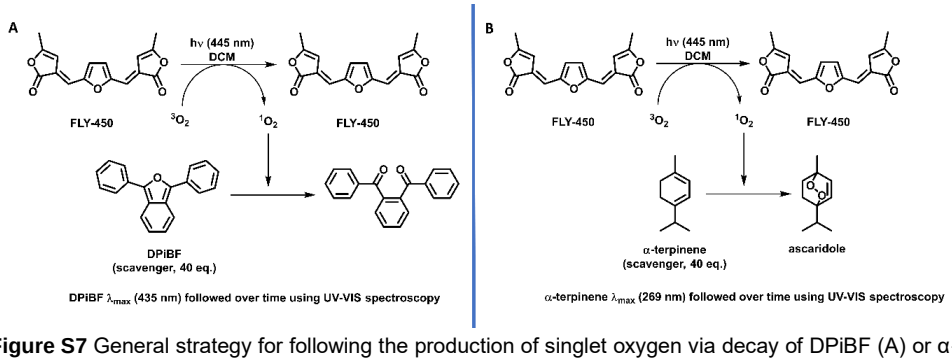

Figure S7 General strategy for following the production of singlet oxygen via decay of DPiBF (A) or α-terpinene (B) over time (s) monitored at the respective main absorption band in MeOH at 293 K.

A 2.0 ml solution containing **FLY 450** (1 µM) along with α-terpinene as a singlet oxygen scavenger (40 µM) in pre-oxygenated DCM or methanol was placed in a 2 mL cuvette. Thereafter, the **FLY 450** + α-terpinene solution was irradiated (λ_{irr} = 445 nm) with a UV/VIS-mounted Sahlmann Photochemical Solutions 445 nm LED system (peak wavelength 445 nm, FWHM 18 nm). During 445 nm irradiation, the solutions' UV/VIS spectrum was monitored for the disappearance of the main absorption band of α-terpinene at 269 nm, signifying consumption of the singlet

oxygen acceptor by the generated singlet oxygen, to produce the graphs shown below (measured as triplicates, single measurements shown in **Figure S8** and **Figure S9**). The rate of singlet oxygen formation was determined at the initial decay of absorbance of α-terpinene at 5% to 20% conversion assuming every molecule of singlet oxygen is captured by the excess of scavenger present. The quantum yield (average of triplicate measurement) was calculated, using methylene blue as the reference compound of which its rate was also determined, following the equations accordingly:

$$A = log_{10}\frac{I_0}{I} \qquad \text{where} \qquad I_0 = 1$$

Gives

$$I = \frac{1}{10^A}$$

where A = absorbance of the photosensitizer at λ_{irr}, I_0 = intensity incident light and I = transmitted intensity. Following from the aforementioned equations the quantum yield (Φ_Δ) is defined as:[45]

$$\Phi_{\Delta\,\mathbf{FLY\,450}} = \frac{I_{Methylene\ blue}}{I_{\mathbf{FLY\,450}}} \times \frac{k_{\mathbf{FLY\,450}}}{k_{Methylene\ blue}} \times \Phi_{\Delta\,\text{Methylene blue}}$$

where *k* = rate of scavenger consumption at λ_{irr}.

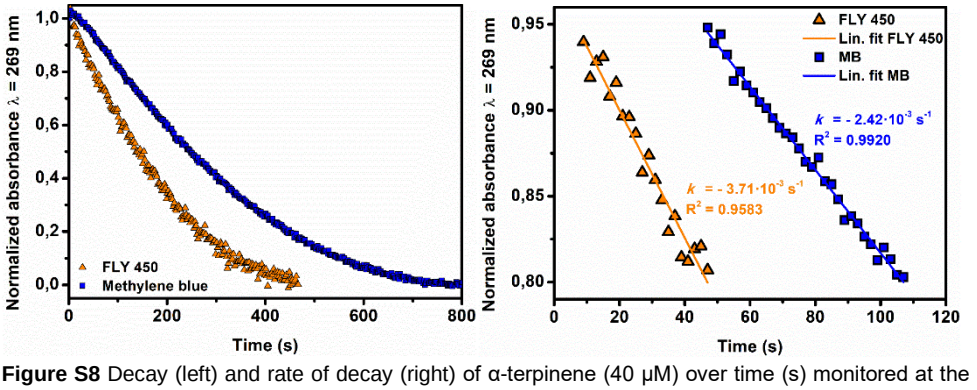

Figure S8 Decay (left) and rate of decay (right) of α-terpinene (40 μM) over time (s) monitored at the main absorption band (λ_{abs} = 269 nm) in MeOH at 293 K. The rate was determined from the initial decay at 5% to 20% conversion.

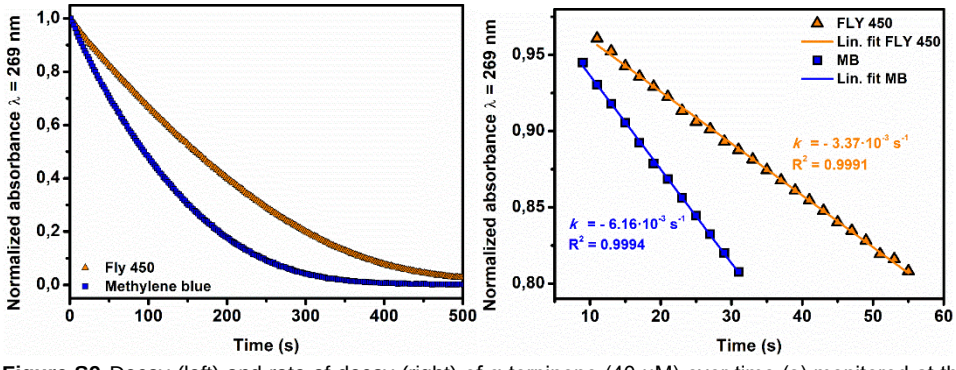

Figure S9 Decay (left) and rate of decay (right) of α-terpinene (40 μM) over time (s) monitored at the main absorption band (λ_{abs} = 269 nm) in DCM at 293 K. The rate was determined from the initial decay at 5% to 20% conversion.

3.6.7 Free radical polymerization kinetics

The reaction kinetics of the copolymerization of methoxybutenolide and dodecyl vinyl ether were determined using ^{1}H NMR spectroscopy. The concentrations of the monomers were followed by integrating the proton NMR signals. To determine the absolute concentration at a certain point, 1,3,5-trimethoxybenzene, an internal standard, was added to the reaction mixture (0.5 eq.). The equations (**Equation S1–S5**, **Chapter 2**, **2.6.4**, *vide supra*) were used to determine the values for ln(1/(1-U)). Plotting these values against t resulted in a linear relation in which the slope of the function is the value for k_{obs}.

For the copolymerization using ascaridole as radical initiator an initial fast rate (k^1_{obs}) followed by a slower secondary rate (k^2_{obs}) is observed (**Figure S12**). Previously we have described these findings in butenolide polymerization reactions as a result of increased inhibition.[26]

^{1}H-NMR shifts that have been followed are ^{1}H NMR (400 MHz, $CDCl_3$): methoxybutenolide δ 6.21 (1H), dodecyl vinyl ether δ 6.43 (1H).

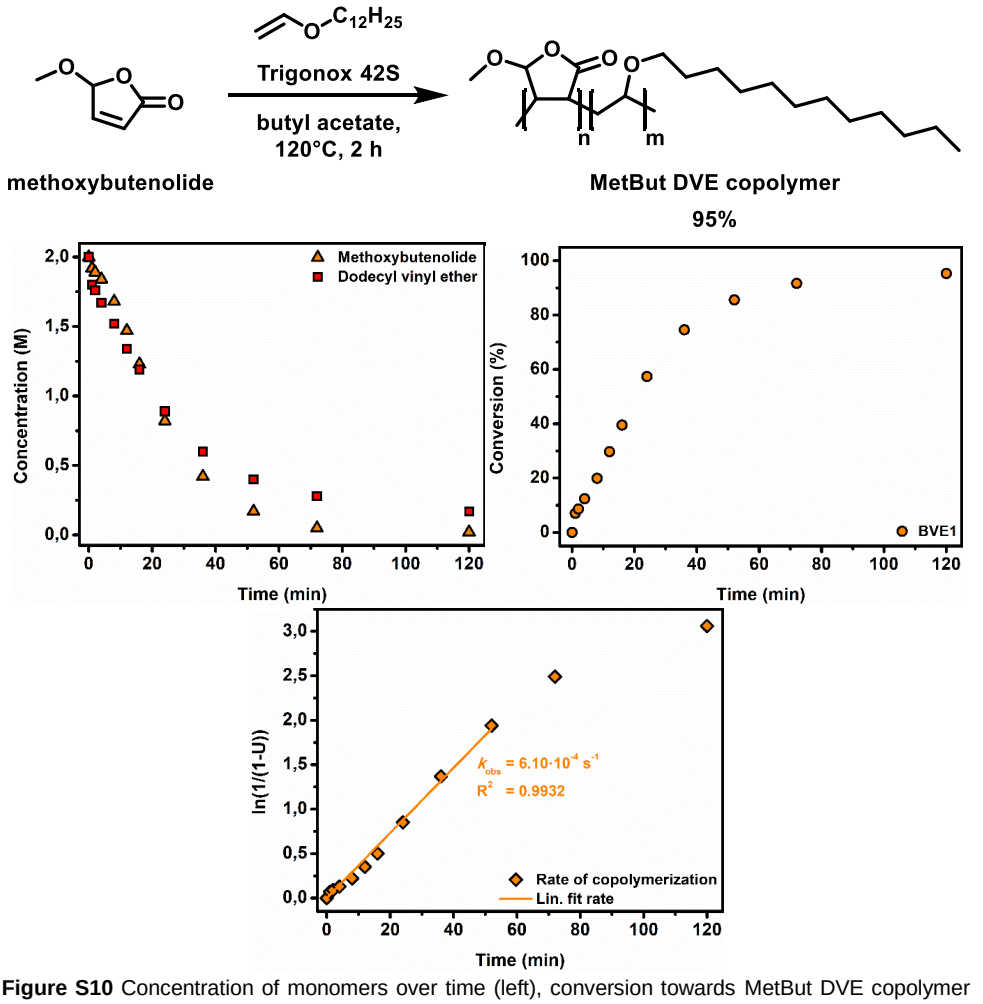

Figure S10 Concentration of monomers over time (left), conversion towards MetBut DVE copolymer **BVE1** over time (right) and the rate of copolymerization (bottom middle) of methoxybutenolide with dodecyl vinyl ether (1:1 ratio) followed by ^{1}H NMR signals over time by taking samples and flash freezing (–18°C) them at certain timestamps and using 1,3,5-trimethoxybenzene (0.5 eq.) as internal standard, reaction conditions: Trigonox 42S (6 mol%), 2 M in butyl acetate 120°C, 2 h.

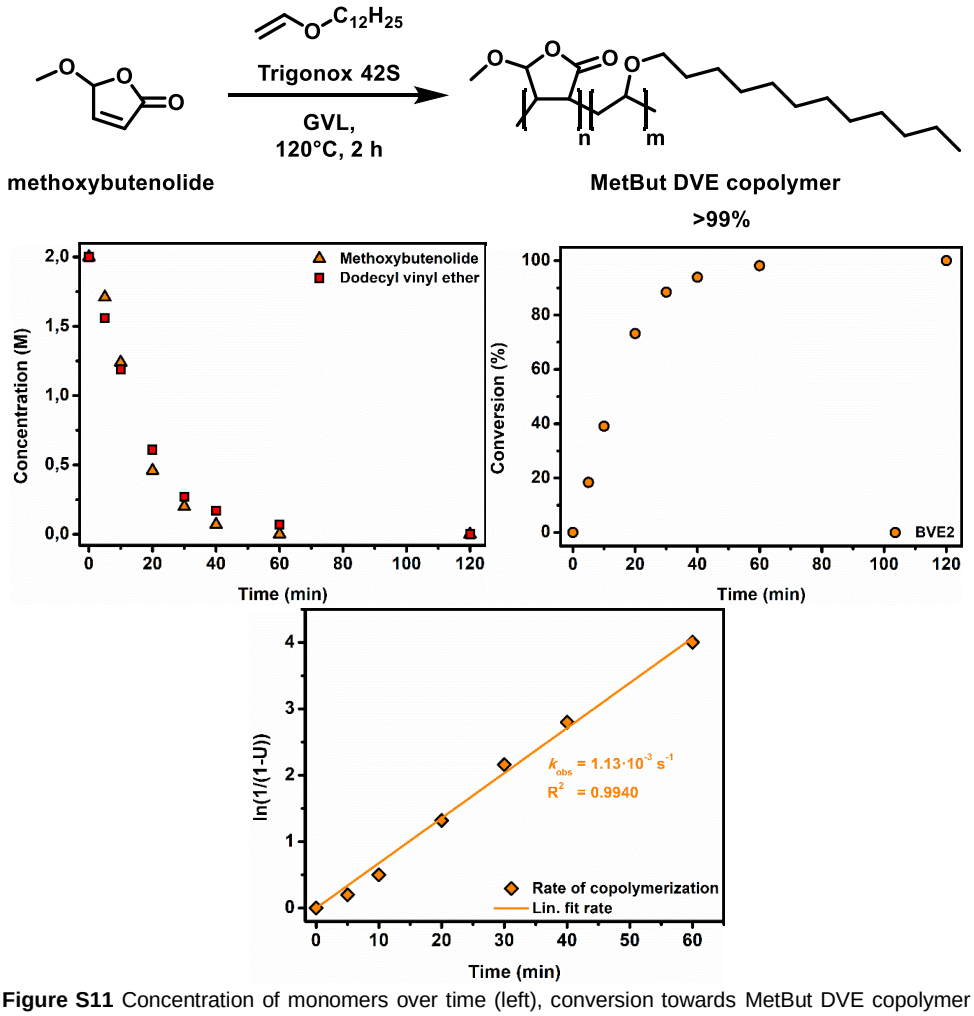

Figure S11 Concentration of monomers over time (left), conversion towards MetBut DVE copolymer **BVE2** over time (right) and the rate of copolymerization (bottom middle) of methoxybutenolide with dodecyl vinyl ether (1:1 ratio) followed by ^{1}H NMR signals over time by taking samples and flash freezing (–18°C) them at certain timestamps and using 1,3,5-trimethoxybenzene (0.5 eq.) as internal standard, reaction conditions: Trigonox 42S (6 mol%), 2 M in GVL 120°C, 2 h.

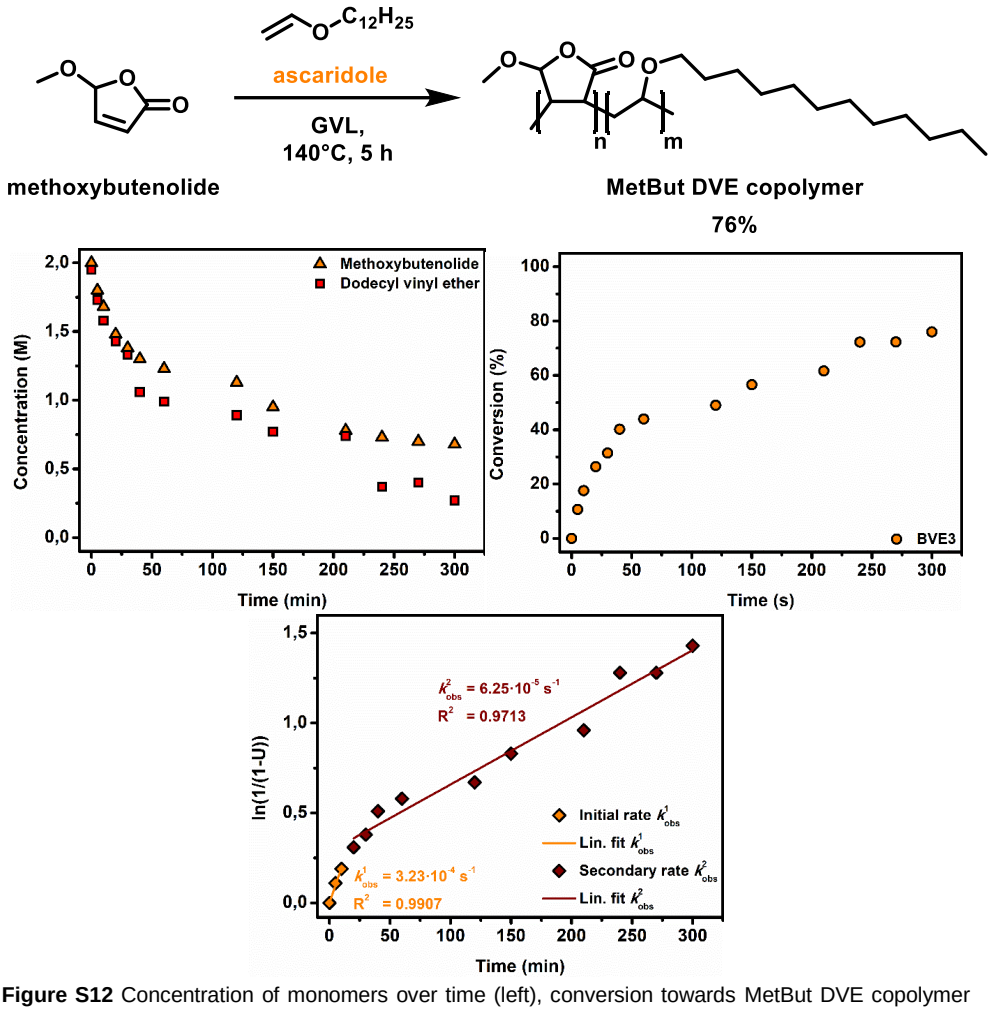

Figure S12 Concentration of monomers over time (left), conversion towards MetBut DVE copolymer **BVE3** over time (right) and the rate of copolymerization (bottom middle) of methoxybutenolide with dodecyl vinyl ether (1:1 ratio) followed by ^{1}H NMR signals over time by taking samples and flash freezing (–18°C) them at certain timestamps and using 1,3,5-trimethoxybenzene (0.5 eq.) as internal standard, reaction conditions: ascaridole (6 mol%), 2 M in GVL 140°C, 5 h.

3.6.8 Methoxybutenolide–1,4-butanedivinyl ether coatings

Following the **UV curing procedure** coatings were prepared using 3 mol% and 6 mol% **VAPO** and 3 mol% **BAPO**. Applying 3 mol% of **VAPO** as photoinitiator resulted in a tacky non-uniform coating (**Figure S13**, left). A higher loading of 6 mol% **VAPO** resulted in a clear hard coating (**Figure S13**, middle). Applying 3 mol% **BAPO** resulted in a hard but opaque coating, presumably caused by unreacted monomers (**Figure S13**, right).

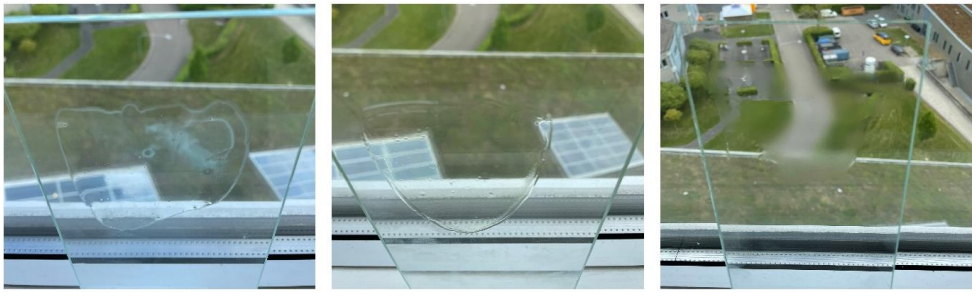

Figure S13 UV cured methoxybutenolide–1,4-butanedivinyl ether coatings using as photoinitiator 3 mol% VAPO (left), 6 mol% VAPO (middle) and 3 mol% BAPO (right). Coating formation conditions: methoxybutenolide–1,4-butanedivinyl ether (1:0.5 ratio), VAPO/BAPO (3–6 mol%), UV irradiation (λ_{irr} = 395 nm), 20 min.

The properly formed methoxybutenolide–1,4-butanedivinyl ether coatings **BVEC1** (6 mol% **VAPO**) and **BVEC2** (3 mol% **BAPO**) were subjected to DSC, Knoop hardness measurement and MEK solvent resistance test (**Figure S14**).

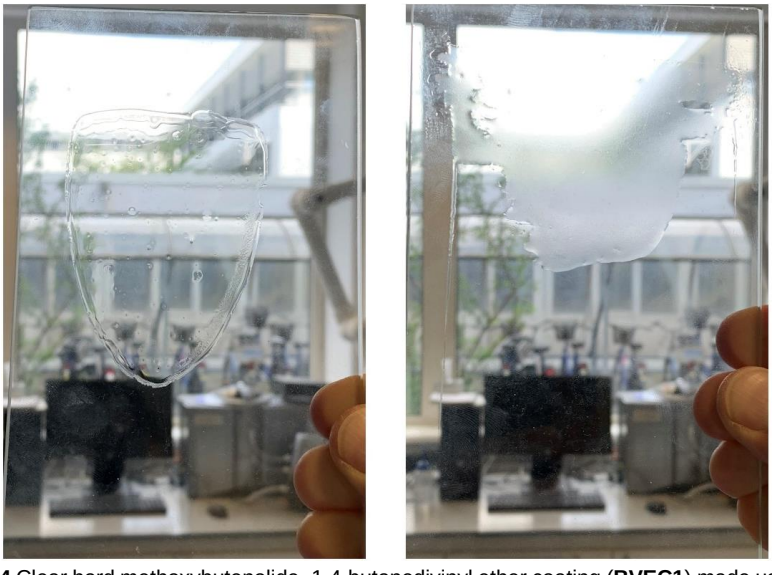

Figure S14 Clear hard methoxybutenolide–1,4-butanedivinyl ether coating (**BVEC1**) made using VAPO (6 mol%) as photoinitiator (left). Hard methoxybutenolide–1,4-butanedivinyl ether coating (**BVEC2**) made using BAPO (3 mol%) as photoinitiator (right).

After subjection of the coatings **BVEC1** and **BVEC2** to the MEK double rub test, where the coatings are rubbed with a soaked cloth in 2-butanone (MEK) back and forth (5 cm) while applying 10 N downward pressure, no apparent damage was present to the surface of the coatings, except for slight whitening (**Figure S15**). The cracking of the coating **BVEC2** was caused by the Knoop hardness experiment performed before the MEK double rub test (**Figure S15**, right). The part of the coating that was subjected to the MEK double rub test is encircled in black.

Figure S15 UV cured methoxybutenolide–1,4-butanedivinyl ether coatings **BVEC1** (left) and **BVEC2** (right) subjected to DSC, Knoop hardness measurement and MEK solvent resistance test. Only slight whitening and no other damage or deterioration of the surfaces was apparent after 200 MEK double rubs.

3.7 References

1. R. A. Sheldon, *Green Chem.*, 2014, **16**, 950-963.
2. M. Beller, G. Centi and L. Sun, *ChemSusChem*, 2017, **10**, 6-13.
3. P. Anastas and N. Eghbali, *Chem. Soc. Rev.*, 2010, **39**, 301-312.
4. P. T. Anastas and J. C. Warner, *Green Chemistry: Theory and Practice*, Oxford University Press, 1998.
5. K. Kohli, R. Prajapati and B. K. Sharma, *Energies*, 2019, **12**, 233.
6. A. K. Mohanty, F. Wu, R. Mincheva, M. Hakkarainen, J.-M. Raquez, D. F. Mielewski, R. Narayan, A. N. Netravali and M. Misra, *Nat. Rev. Methods Primers*, 2022, **2**, 46.
7. T. Ohara, T. Sato, N. Shimizu, G. Prescher, H. Schwind, O. Weiberg, K. Marten, H. Greim, T. D. Shaffer and P. Nandi, in *Ullmann's Encyclopedia of Industrial Chemistry*, Wiley-VCH, Weinheim, 2020, Acrylic Acid and Derivatives, 1-21.
8. M. M. Lin, *Appl. Catal. A: Gen*, 2001, **207**, 1-16.
9. R. Höfer and M. Selig, in *Polymer Science: A Comprehensive Reference*, eds. K. Matyjaszewski and M. Möller, Elsevier, Amsterdam, 2012, vol. 10, ch. 2 Green Chemistry and Green Polymer Chemistry, 5-14.
10. H. Lutz, H. P. Weitzel and W. Huster, in *Polymer Science: A Comprehensive Reference*, eds. K. Matyjaszewski and M. Möller, Elsevier, Amsterdam, 2012, vol. 10, ch. 27 Aqueous Emulsion Polymers, 479-518.
11. D. Urban and D. Distler, in *Polymer Dispersions and Their Industrial Applications*, eds. D. Urban and D. Distler, Wiley-VCH, Weinheim, 2002, ch. 1 Introduction, 1-14.
12. R. Schwalm, in *Polymer Science: A Comprehensive Reference*, eds. K. Matyjaszewski and M. Möller, Elsevier, Amsterdam, 2012, vol. 10, ch. 30 Radiation-Curing Polymer Systems, 567-579.
13. G. Crapper, in *Polymer Science: A Comprehensive Reference*, eds. K. Matyjaszewski and M. Möller, Elsevier, Amsterdam, 2012, vol. 10, ch. 29 Powder Coatings, 541-566.
14. R. Höfer, in *Sustainable Solutions for Modern Economies*, The Royal Society of Chemistry, London, 2009, ch. 1 History of the Sustainability Concept – Renaissance of Renewable Resources, 1-11.
15. J. B. Zimmerman, P. T. Anastas, H. C. Erythropel and W. Leitner, *Science*, 2020, **367**, 397-400.
16. A. Z. Yu, J. M. Sahouani and D. C. Webster, *Prog. Org. Coat.*, 2018, **122**, 219-228.
17. F. Diot-Néant, E. Rastoder, S. A. Miller and F. Allais, *ACS Sustain. Chem. Eng.*, 2018, **6**, 17284-17293.
18. M. Moreno, M. Goikoetxea, J. C. de la Cal and M. J. Barandiaran, *J. Polym. Sci., Part A: Polym. Chem.*, 2014, **52**, 3543-3549.

19. J. T. Trotta, M. Jin, K. J. Stawiasz, Q. Michaudel, W.-L. Chen and B. P. Fors, *J. Polym. Sci., Part A: Polym. Chem.*, 2017, **55**, 2730-2737.
20. S. Pérocheau Arnaud, E. Andreou, L. V. G. Pereira Köster and T. Robert, *ACS Sustain. Chem. Eng.*, 2020, **8**, 1583-1590.
21. S. Okada and K. Matyjaszewski, *J. Polym. Sci., Part A: Polym. Chem.*, 2015, **53**, 822-827.
22. T. Okuda, K. Ishimoto, H. Ohara and S. Kobayashi, *Macromolecules*, 2012, **45**, 4166-4174.
23. G. Quintens, J. H. Vrijsen, P. Adriaensens, D. Vanderzande and T. Junkers, *Polym. Chem.*, 2019, **10**, 5555-5563.
24. I. Khalil, G. Quintens, T. Junkers and M. Dusselier, *Green Chem.*, 2020, **22**, 1517-1541.
25. D. Esposito and M. Antonietti, *Chem. Soc. Rev.*, 2015, **44**, 5821-5835.
26. J. G. H. Hermens, T. Freese, K. J. v. d. Berg, R. v. Gemert and B. L. Feringa, *Sci. Adv.*, 2020, **6**, eabe0026.
27. A. Jaswal, P. P. Singh and T. Mondal, *Green Chem.*, 2022, **24**, 510-551.
28. K. Noweck and W. Grafahrend, in *Ullmann's Encyclopedia of Industrial Chemistry*, Wiley-VCH, Weinheim, 2006, Fatty Alcohols, 117-141.
29. J. S. Wau, M. J. Robertson and M. Oelgemöller, *Molecules*, 2021, **26**, 1685.
30. J. J. Bozell and G. R. Petersen, *Green Chem.*, 2010, **12**, 539-554.
31. F. Ronzani, N. Costarramone, S. Blanc, A. K. Benabbou, M. L. Bechec, T. Pigot, M. Oelgemöller and S. Lacombe, *J. Catal.*, 2013, **303**, 164-174.
32. D. M. Alonso, S. G. Wettstein and J. A. Dumesic, *Green Chem.*, 2013, **15**, 584-595.
33. A. Burgard, M. J. Burk, R. Osterhout, S. Van Dien and H. Yim, *Curr. Opin. Biotechnol.*, 2016, **42**, 118-125.
34. J. Saska, Z. Li, A. L. Otsuki, J. Wei, J. C. Fettinger and M. Mascal, *Angew. Chem. Int. Ed.*, 2019, **58**, 17293-17296.
35. A. Gualandi, M. Anselmi, F. Calogero, S. Potenti, E. Bassan, P. Ceroni and P. G. Cozzi, *Organic & Biomolecular Chemistry*, 2021, **19**, 3527-3550.
36. S. Xu, Y. Yuan, X. Cai, C.-J. Zhang, F. Hu, J. Liang, G. Zhang, D. Zhang and B. Liu, *Chem. Sci.*, 2015, **6**, 5824-5830.
37. H. S. Yu, X. He, S. L. Li and D. G. Truhlar, *Chem. Sci.*, 2016, **7**, 5032-5051.
38. J. Zheng, X. Xu and D. G. Truhlar, *Theor. Chem. Acc.*, 2011, **128**, 295-305.
39. A. V. Marenich, C. J. Cramer and D. G. Truhlar, *J. Phys. Chem. B*, 2009, **113**, 6378-6396.
40. F. Wilkinson, W. P. Helman and A. B. Ross, *J. Phys. Chem. Ref. Data*, 1993, **22**, 113-262.
41. C. A. Clark, D. S. Lee, S. J. Pickering, M. Poliakoff and M. W. George, *Org. Process Res. Dev.*, 2016, **20**, 1792-1798.
42. J. G. H. Hermens, A. Jensma and B. L. Feringa, *Angew. Chem. Int. Ed.*, 2022, **61**, e202112618.
43. R. W. Redmond and J. N. Gamlin, *Photochem. Photobiol.*, 1999, **70**, 391-475.
44. U. Yoshiharu, *Chem. Lett.*, 1973, **2**, 743-744.
45. L. V. Lutkus, S. S. Rickenbach and T. M. McCormick, *J. Photochem. Photobiol. A: Chem.*, 2019, **378**, 131-135.
46. C. Capello, U. Fischer and K. Hungerbühler, *Green Chem.*, 2007, **9**, 927-934.
47. E. Kirillov, K. Rodygin and V. Ananikov, *Eur. Polym. J.*, 2020, **136**, 109872.
48. W. Reppe, *Production of vinyl ethers*, US1959927A, 1931.
49. S. P. Teong and Y. Zhang, *J. Bioresour. Bioprod.*, 2020, **5**, 96-100.
50. K. S. Rodygin, M. S. Ledovskaya, V. V. Voronin, K. A. Lotsman and V. P. Ananikov, *Eur. J. Org. Chem.*, 2021, **2021**, 43-52.
51. Z. Li, Z. Liu, R. Wang, X. Guo and Q. Liu, *Chem. Eng. Sci.*, 2018, **192**, 516-525.
52. S. P. Teong, A. Y. H. Chua, S. Deng, X. Li and Y. Zhang, *Green Chem.*, 2017, **19**, 1659-1662.
53. K. S. Rodygin, I. Werner and V. P. Ananikov, *ChemSusChem*, 2018, **11**, 292-298.
54. G. Werner, K. S. Rodygin, A. A. Kostin, E. G. Gordeev, A. S. Kashin and V. P. Ananikov, *Green Chem.*, 2017, **19**, 3032-3041.
55. R. Zand and R. B. Mesrobian, *J. Am. Chem. Soc.*, 1955, **77**, 6523-6524.
56. *Initiators for thermoplastics*, Nouryon, https://www.nouryon.com/globalassets/inriver/resources/brochure-initiators-for-thermoplastics-feb2021-en_us.pdf, 2021 (accessed on 10/07/2022).
57. L. Breloy, C. Negrell, A. S. Mora, W. S. J. Li, V. Brezová, S. Caillol and D. L. Versace, *Eur. Polym. J.*, 2020, **132**, 109727.
58. K. J. van den Berg, L. G. J. van der Ven and H. J. W. van den Haak, *Prog. Org. Coat.*, 2008, **61**, 110-118.
59. D. E. Fiori, D. A. Ley and R. J. Quinn, *J. Coat. Technol.*, 2000, **72**, 63-69.
60. J. A. Howard and G. D. Mendenhall, *Can. J. Chem.*, 1975, **53**, 2199-2201.


Gloss
RAL
9010
HOOGGLANS